Micromechanisms of fracture in nodular cast iron: From experimental findings towards modeling strategies – A review

Geralf Hütter, Lutz Zybell, Meinhard Kuna

Micromechanisms of fracture in nodular cast iron: From experimental findings towards modeling strategies — A review.

Article published in Engineering Fracture Mechanics, 144(2015), 118–141. The final publication is available at www.sciencedirect.com, doi:10.1016/j.engfracmech.2015.06.042

Geralf Hütter, Lutz Zybell, Meinhard Kuna

This article presents an overview on modeling of micromechanical failure processes in nodular cast iron, a material used for many engineering applications. Depending on the loading conditions, different micromechanisms are responsible for damage and failure of nodular cast iron. The scope of this article is to derive a connection between experimental findings and simulation approaches for those different micromechanisms. Based on a review of experimental studies, the models are classified by several criteria into different modeling strategies. The main findings achieved for homogeneous stress states as well as for fracture and machining simulations are summarized and compared. *Keywords:* nodular cast iron; damage mechanisms; modeling; micromechanics simulations; finite elements

1 Introduction

Nodular cast iron[1] (NCI), also known as spheroidal graphite cast iron, is a carbon-rich iron alloy. Due to the high carbon content, graphite is found as particles on the microstructure level embedded into the metallic matrix. The term "nodular" refers to the shape of the graphite particles which is achieved by certain alloying elements like magnesium. Compared to classical gray cast iron with lamellar graphite, the nodular particle shape increases strength and toughness becoming comparable to many grades of steel. In addition, the cost-effective casting production allows a high design flexibility which is why nodular cast iron is widely used in industry, e.g. for gearboxes, crankshafts, pipes or nuclear storage and transportation casks.

The nodular graphite particles have a volume fraction between 7% and 15% and exhibit typically a diameter d_G in the range between 10 µm and 150 µm. They thus constitute strong heterogeneities in the microstructure affecting the macroscopic mechanical properties. Size, (deviations from the spherical) shape and distribution of graphite particles and the microstructure of the metallic matrix depend on temperature evolution during the casting process and possible subsequent heat treatments. Especially in thick-walled casted components the local temperature evolutions at the surface and in the center can differ considerably resulting in locally different microstructures and thus in locally varying mechanical properties.

[1] Due to its mechanical properties nodular cast iron is also known as "ductile cast iron (DCI)". However, in order to avoid confusion with the damage mechanisms which will be discussed below, this term is omitted here.

Of course, then the question arises whether the local strength or toughness is sufficient to sustain the local loading conditions — or other the way round: Which microstructure has to be adjusted by (additional) heat treatments to make the component resist the local loading conditions? Answering these questions requires that a relation between microstructure and macroscopic mechanical properties can be drawn. This relation has been subject of both experimental and computational investigations. The latter approach becomes more and more powerful with increasing computing power. Furthermore, NCI is an ideal material for this approach since the geometry of the microstructure can be easily determined by optical imaging and, as mentioned before, can be influenced specifically. That is why the present paper aims in providing a review on the current state of the art of the modeling of micromechanics of NCI pointing out the specifics of this material. Reviews on the applications and properties of NCI were published on occasion of 50 years of applications of NCI [70] and from German [9] and Japanese points of view [63]. A review on fracture testing of cast iron materials was given recently [96]. Reviews on the modeling of other engineering metals, typically steels and light-weight alloys, can be found elsewhere [16, 95, 116].

The outline of the present paper is as follows: In Section 2 some experimental results are reviewed briefly as they are necessary for an accurate modeling, before in Section 3 the available models are classified according to several criteria. Then, the classes of models are discussed in Sections 4 and 5 before we close with a summary and outlook.

2 Experimental characterization

2.1 Classification

The classification of NCI is defined in the standards EN-1563 [33] and ASTM A536 [4]. In both systems the grade code number is related to ultimate strength (MPa resp. ksi) and percent elongation at fracture. Both quantities depend on the microstructure of the metallic matrix and on the shape of the graphite particles. The matrix material can have a ferritic, pearlitic or austenitic structure or intermediate stages depending on the chemical composition of the matrix and on the heat treatment as shown in Figure 1. In ferritic-pearlitic NCIs, a so-called "bulls eye" structures of ferrite can be found around the graphite particles, see Figure 1b. By additional heat treatment the matrix material can be transformed into bainite consisting of needle shaped ferrite and austenite. This material is known as austempered ductile iron (ADI).

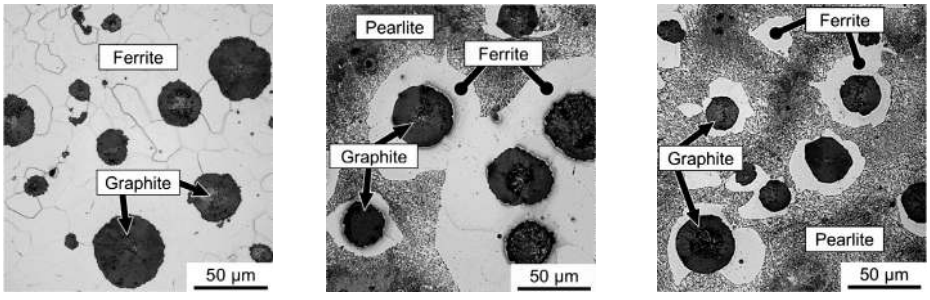

(a) (b) (c)

Figure 1: Different kinds of nodular cast iron (NCI) (from [34]): a) ferritic NCI b) ferritic-pearlitic NCI with so-called "bulls eye" structures c) pearlitic NCI

2.2 Stereology of NCI microstructures

In order to quantify the influence of the microstructure on the properties of NCI, one needs to define corresponding geometric measures of the statistical microstructure of NCI. Basic geometric quantities of NCI are the relative number of graphite particles (2D: N_A the mean number per unit area, 3D: N_V the mean number per unit volume), graphite volume fraction f_0 and a mean distance λ between centers of neighboring graphite particles These quantities can be obtained by statistical evaluation of 2D images from micrographs or from 3D images. The probably most prominent stereological method is closely related to the solution of Wicksell's corpuscle problem, namely the stereological estimation of the diameter distribution function of the spheres from the diameter distribution function of the section circles observed in a metallographic cross section [83, 91]. A further problem is the characterization of the 3D arrangement of the graphite particles, which can be expressed in terms of the pair correlation function of the spheres' centers. A stereological method of estimating the pair correlation function of the spheres' centers from the pair correlation function of the section circles is presented in [47].

However, for practical applications it is usually not necessary to determine the complete distribution and correlation functions. Rather, it is desirable to establish links between mechanical properties of NCI and mean measures of its microstructure like the above-mentioned λ, f_0, N_A and N_V. The latter three quantities are related to each other by

$$f_0 = N_V \overline{V},\ f_A = f_0,\ N_A = 2\overline{R} N_V,\ \ \overline{V} = \alpha_V \left(2\overline{R}\right)^3 . \tag{1}$$

Therein, $\overline{R}$ and $\overline{V}$ denote the mean values of the particle radii and volumes, respectively. Furthermore, f_A is the area fraction of the graphite particles in a micrograph. Remarkably, f_A equals the volume fraction f_0 independent of the particular distribution of radii. The factor α_V accounts for the fact that the mean of the cubed diameter of the particles differs in general from the cube of the mean diameter and depends thus on the particular distribution function. For practically relevant distributions $\alpha_V \approx 1$ (e.g. $\alpha_V = 1$ for a Rayleigh distribution, $\alpha_V = \pi/3$ for a uniform distribution). Only if all particles have the same diameter, a smaller value of $\alpha_V = \pi/6$ is obtained.

The mean particle distance λ can be characterized by different measures. In the mathematical literature and software packages built thereupon mostly the *mean distance λ_{nn} between nearest neighbors* is employed for this purpose. However, in the light of the mostly ductile failure mechanisms of NCI acting always over several neighboring particles (as will be discussed in detail in Section 5.1), a measure taking into account all neighbors is more appropriate. That is why in [58]

$$\lambda = 1/\sqrt[3]{N_V} \tag{2}$$

was defined as adequate measure of the mean distance of graphite particles corresponding effectively to the lattice constant of a regular cubic-primitive arrangement of same density N_V. Using Eq. (1), this definition yields $\lambda = \left(f_0/\alpha_V\right)^{1/6} / \sqrt{N_A}$ allowing to compute λ from measures N_A and $f_0 = f_A$ which can be directly determined from micrographs. The influence of the particular distribution of radii is relatively weak since α_V is close to one and enters only in the sixth root. A similar approach $\lambda = 0.5/\sqrt{N_A}$ was proposed by Salzbrenner [102]. The ratio between the mean distance according to Eq. (2) and the mean nearest-neighbor distance λ_{nn} depends considerably on the pair correlation function of the particles' centers. For instance, if the particles are regularly arranged the ratio is $\lambda_{\mathrm{nn}}/\lambda = 1$ whereas the values $\lambda_{\mathrm{nn}}/\lambda = 0.55$ and $\lambda_{\mathrm{nn}}/\lambda = 0.62$ are obtained if the centers are assumed to originate from stationary Poisson point processes or from Matérn's hard-core point processes, respectively. For details we refer to Ohser and Mücklich [91].

The graphite particle distance λ and the graphite particle size (mean radius $\overline{R}$ or mean diameter d_{G}, resp.) scale to each other for a fixed graphite volume fraction of $f_0 \approx 0.07 \ldots 0.15$ by

$$\frac{\overline{R}}{\lambda} = \sqrt[3]{\frac{3f_0}{4}} \approx 0.37 \ldots 0.48. \tag{3}$$

So conclusions drawn with respect to graphite particle size $\overline{R}$ are valid as well with respect to graphite particle distance λ. Additionally, a similar scaling holds for the size of the ferrite grains.

Extensive research has also been done in characterizing the shape of the graphite particles, for classification see e.g. [61]. Thereby, the so-called shape factor $f = 4\pi A/U^2$, with A being the area of a graphite particle in a plane section and U its circumference, is a measure of the nodularity of the graphite particles. Modern techniques like scanning electron microscopy (SEM) with focused ion beam (FIB) thinning [122] allow for a precise determination of this measure, which is of important concern for the field of non-spheroidal graphite cast irons such as e.g. gray cast iron containing lamellar graphite.

2.3 Macroscopic mechanical behavior

Due to the embedded graphite particles, the macroscopic behavior of NCI under different loading conditions is different from common steels and will be discussed with respect to the influence of the specific microstructure in the following.

2.3.1 Monotonic loading

Under monotonic tension loading NCI shows no distinct yield point. Furthermore, there is a tension-compression asymmetry, with the yield stress in compression being larger than in tension up to 7% [43, 49, 78]. The strength and the hardening behavior of NCI are strongly influenced by the matrix material properties showing a ratio of yield stress to ultimate strength of about 0.65...0.75. As for the very most engineering metals, the yield stress of NCI increases with increasing rates of loading, decreasing temperature and decreasing grain size (Hall-Petch effect). In ferritic-pearlitic NCIs the yield stress increases also with increasing content of pearlite and increasing contents of silicon. Also the strain to fracture depends strongly on the microstructure and chemical composition. With higher content of pearlite, and/or stronger deviations of the shape of the graphite particles from the spherical one, and/or higher contents of silicon the material becomes more brittle and thus the strain at failure decreases. Empirical relations for the effect were derived by Nilsson et al. [89, 90]. Especially under low stress triaxialities the graphite plays an important role, which was, however, only investigated in a few studies yet [26, 78].

Nodular cast irons with a body-centered cubic matrix (ferrite, pearlite, bainite) exhibit a ductile-to-brittle transition (DBT) with decreasing temperature and/or increased rates of loading. The DBT temperature depends on the microstructure, if the pearlite content is larger than 50 % [66], and on the chemical composition, especially on the content of silicon [96]. However, for NCI the characteristic drop of the Charpy energy with decreasing temperature appears over a wider temperature range than for comparable ferritic steels [9].

Regarding fracture testing of NCI, "general consensus of the criteria for crack initiation has not been reached" yet [63] due to the inhomogeneous microstructure of NCI. Current studies utilize the concept of a so-called "stretch-zone" (e.g. [7, 65, 124]), but an exact definition of respective measures is not trivial either, especially in the DBT regime [96].

Nevertheless, the correlation of fracture toughness and microstructure is of great practical interest and has thus been intensively studied (with different measures of the fracture toughness). Figure 2 shows the compiled fracture toughness values for ferritic NCIs in the ductile regime with different values λ of the mean distance of the graphite particles. The data can adequately be described empirically by a linear interrelationship with offset as proposed also by Salzbrenner [102] and Pusch et al. [96].

The influence of the microstructure of the matrix on the fracture toughness was also investigated intensively. In general, it is found that higher contents of pearlite and martensite lead to higher strengths at the expense of lower fracture toughness values, see Figure 3. Detailed overviews about fracture mechanics properties of different types of NCI are given in [9, 13, 96]. In addition, numerous fracture tests under increased rates of loading were performed with several techniques [6, 8, 96, 113, 125].

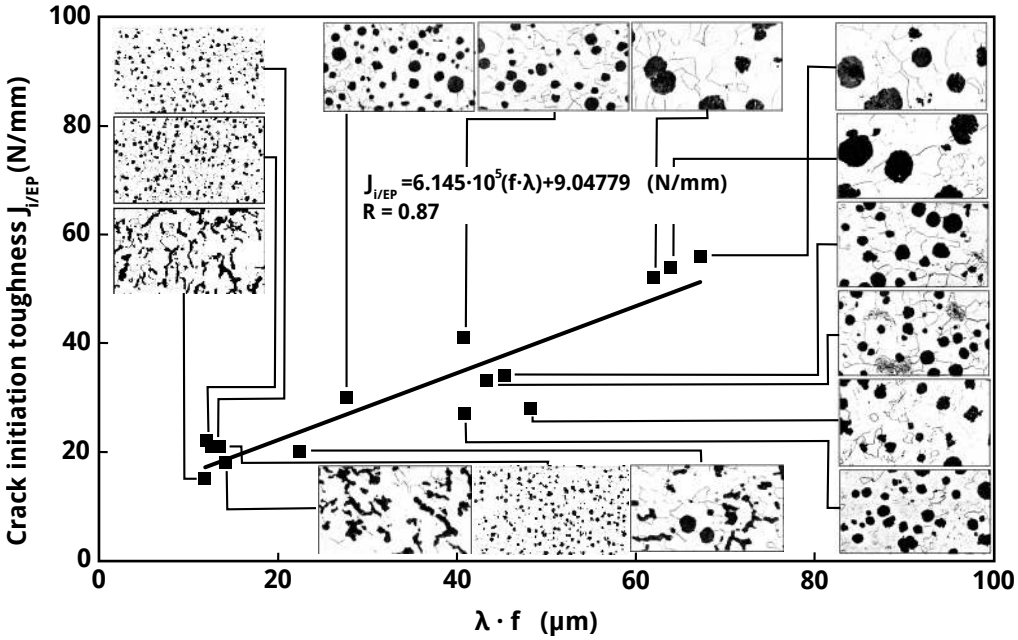

Figure 2: Correlation of fracture toughness J_c vs. graphite particle distance λ times shape factor f for ferritic NCIs EN-GJS-400 (from [5])

Such tests are relevant for engineering applications but impose the severe practical problem especially the determination of the current crack length.

2.3.2 Cyclic loading and fatigue

As mentioned before, NCI exhibits a tension-compression asymmetry with a larger compressive yield stress. Under cyclic loading there is a specific Bauschinger effect characterized by a high internal stress and an unusual hysteresis loop if the accumulated plastic strain is smaller than 100 %. This is mainly caused by interactions between matrix and graphite particles. The Bauschinger effect reduces with further cycling when plastification takes place predominantly in the matrix material [43]. The cyclic behavior already stabilizes after 15 cycles and the parameters for the isotropic-kinematic hardening are not much influenced by different microstructure of matrix or graphite particles, resp. [134].

Fatigue properties of NCI and the correlation to microstructural parameters were investigated by a number of researchers [25, 81, 98]. They found a strong relation between graphite particle size and fatigue life. Also cyclic loading with variable amplitudes [35] and loading in the VHCF regime [128] were investigated. A comprehensive database for HCF behavior of NCI of type EN-GJS-400 including a study on the influence of casting defects on fatigue life is given in [107]. Common to all cited studies is the finding, that the fatigue life of NCI is governed by the size of a single graphite particle or casting defect, resp., from where the fatigue crack initiates. Recently, the field of multi-axial fatigue of NCI also attained attraction [15, 34].

Regarding the short crack behavior of NCI on the microstructural level, it was found by Palin-Luc et al. [92], that ferritic-pearlitic NCIs with bulls-eye structure exhibit micro-cracks within the matrix, which arrest at the ferrite/pearlite interface, at a stress level equal to the conventional endurance limit. These microcracks do not interact directly with each other. However, they lead to macroscopic changes of the unloading stiffness. Thus, another limit can be defined below the conventional endurance one, where micro-cracks do not initiate in the matrix. Furthermore it was found by Endo and Yanase [34]

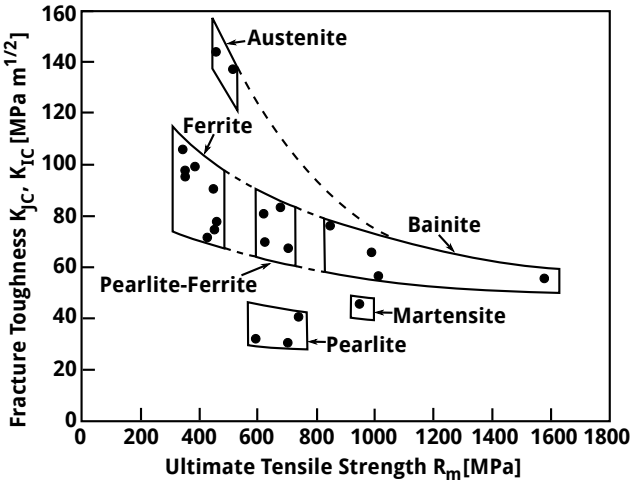

Figure 3: Influence of the microstructure of the matrix on fracture toughness and ultimate tensile strength at room temperature (from [126])

that these micro-cracks do not interact.

Thermo-mechanical fatigue of NCI is of important concern for automotive combustion engine components. This topic was investigated by Seifert et al. [104] and Mellouli et al. [77]. They found that the tension-compression asymmetry appears only at large strains. A microstructure with smaller graphite particles increased the number of cycles to crack initiation and decreased the crack numbers and the main crack growth rate. Furthermore, it was found by Metzger et al. [79] that an additional cyclic loading in the HCF regime superimposed to the thermo-mechanical one leads to a reduced lifetime if a certain threshold of the amplitudes is exceeded.

2.3.3 Fatigue crack growth

Besides cracks on the microlevel, also macroscopic cracks are important for dimensioning of components under cyclic loading. These macroscopic cracks may represent casting defects or may evolve from coalesced microcracks. There exist a huge amount of fatigue crack growth data for NCI in the literature [13, 50, 96, 129, 134], but restricted to positive stress ratios only. Thereby, the Paris regime is mostly independent of the material microstructure. There is only a small influence of the graphite particle distance on the threshold value and the critical cyclic stress intensity factor [81, 96]. Furthermore, by applying statistical quantile crack growth curves, a procedure for obtaining conservative safety assessment results was developed [48, 96] by using the NASGRO equation. With modern X-ray tomography [72, 73, 123], where the graphite particles are used as markers, it is possible to analyze the formation of small fatigue cracks in a restricted volume of one or two mm^3 up to µm-precision. Combining this technique with numerical simulation, it is possible to obtain local crack driving forces and closure levels. Latest achievements in the investigation of fatigue cracks are studies of 3D semi-elliptical surface cracks by *in situ* tomography [71] and 3D observation of real casting defects [24]

2.4 Micromechanisms

2.4.1 Monotonic loading

Under monotonic static loading at room temperature, NCI mainly fails by a ductile mechanism. Thereby the graphite particles start to debond from the metallic matrix when the macroscopic yield strength

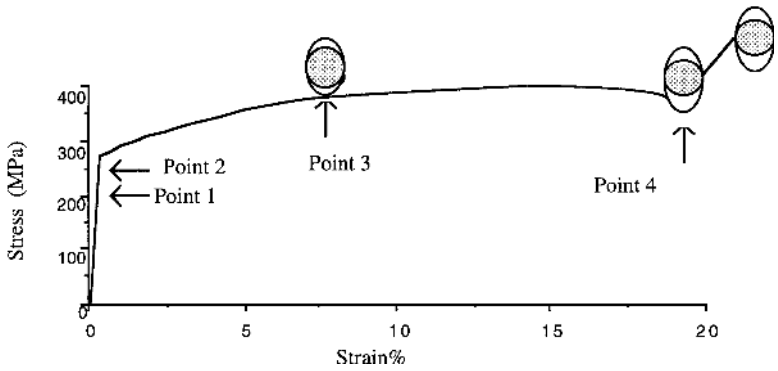

(a)

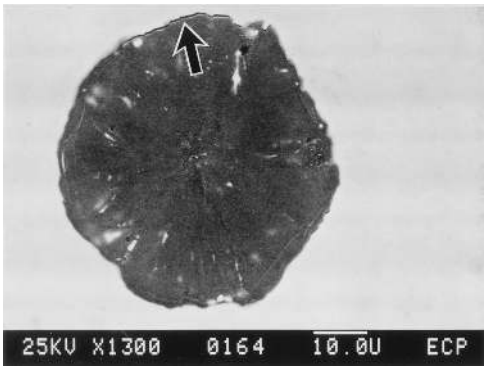

(b)

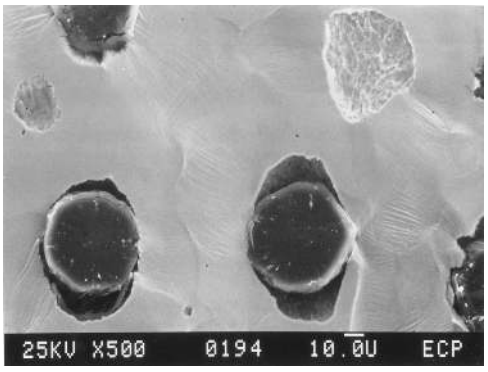

(c)

Figure 4: Ductile mechanism in NCI for a tensile test (from [31]): (a) macroscopic stress-strain curve, (b) debonding of graphite particles at point 2, (c) growth of voids at point 3 (point 1: first microscopic plastification, point 4: final failure)

is reached, see Fig. 4. Subsequently, the formed voids grow with increasing plastic straining. Finally, void growth turns into void coalescence by failure of the intervoid ligaments within a very localized region [31, 40]. Further details of this void nucleation and growth process in NCI including measured parameters can be found in [44]. The void growth process is also influenced by the initial void shape [74].

Debonding of graphite particles, growth of the thereby created voids and finally void coalescence are also the processes that are observed in front of the crack tip during fracture testing as shown in Figure 5. However, the strongly elongated shape of the voids prior to coalescence from tensile tests (Figure 4c) is not observed in the fracture process zone (Figure 5c) due to the larger hydrostatic stresses there. Furthermore, Figure 5 shows that graphite particles do not debond only directly in the crack plane but also in a region around.

Consequently, typical fracture surface of NCI (see Fig. 6) exhibit the following features: Large primary voids are located around the graphite particles. Depending on the matrix material the intervoid ligaments either fail by cleavage (preferably the pearlitic grains and favored also by deviations of the particles from the spherical shape) or by a ductile mechanisms. A broad overview of different fracture surfaces of NCI and the associated mechanisms can be found in [76]. Therein, it is documented additionally, that cleavage fracture in ferritic-pearlitic NCI tends to initiate at the inclusions around the eutectic cell boundary rather than at the graphite-matrix interface. However, locally limited cleavage

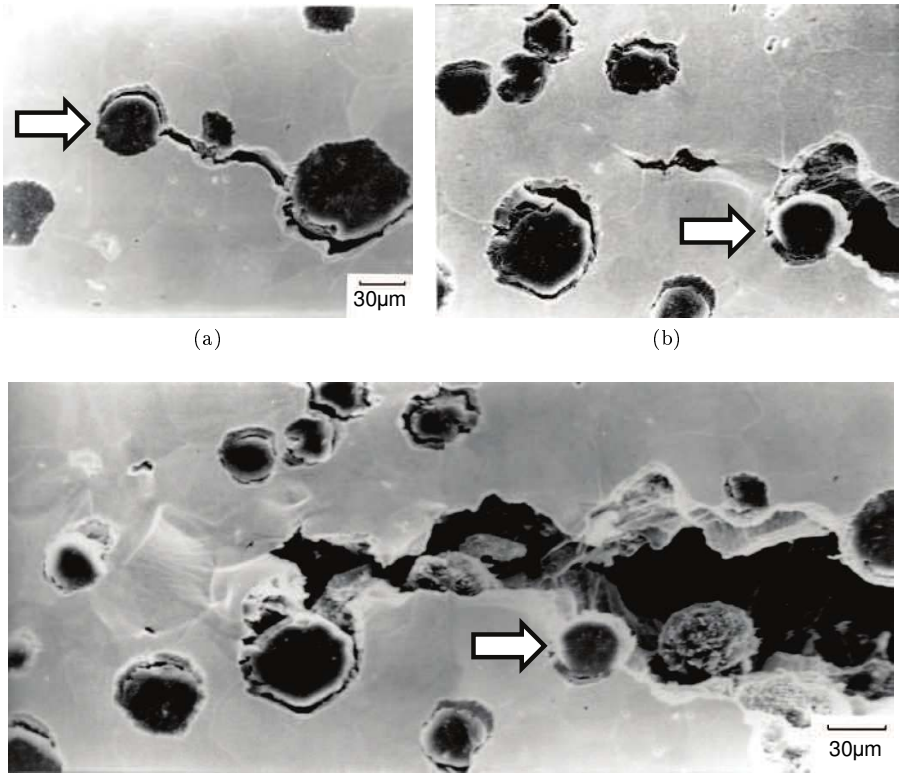

(a) (b)

(c)

Figure 5: Ductile mechanism in NCI for a fracture test (initial crack tip marked with an arrow; from [96]): (a) begin of crack opening, (b) debonding of graphite particles in front of the crack tip, (c) crack propagation

initiation in NCI in the DBT regime does not lead to a severe drop of the fracture toughness as observed e.g. with ferritic steels [9, 101, 108]. Furthermore, the macroscopic crack propagation in NCI can remain stable (macroscopically apparently ductile) despite local cleavage events [96]. In the upper-shelf regime, the ductile mechanism is influenced by the spatial distribution of the interacting voids: If the voids are closely spaced, void coalescence takes place by internal necking of the intervoid ligaments, leaving small secondary voids (one order of magnitude smaller than the primary ones) at the ridges of the primary dimples. If the primary voids and the resulting dimples are wider spaced, secondary voids nucleate from small non-metallic inclusions (MnS, Al_2O_3, CaO) in the matrix material [40, 74], see Fig. 6d.

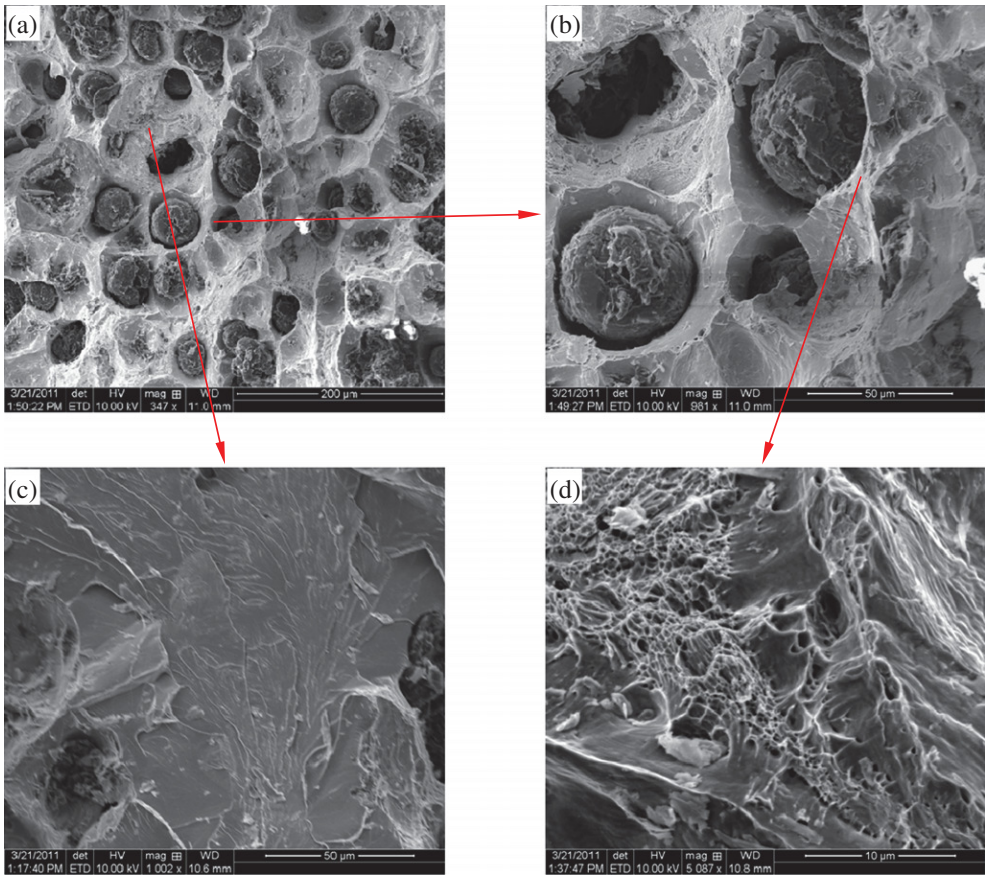

Figure 6: Fracture surface of ferritic-pearlitic NCI under monotonic static loading (from [40]): a) fracture surface with b) primary dimples originating from graphite particles, c) local transgranular cleavage and d) secondary voids on ridges between primary dimples

2.4.2 Cyclic loading

Guillemer-Neel et al. [43] investigated the dislocation evolution in NCI during cyclic loading. They found that dislocation arrangements during strengthening are in accordance to α-iron or Fe-Si polycrystals. Furthermore, the before-mentioned specific Bauschinger effect is caused by inhomogeneous deformations between particles and matrix and by the development of enhanced dislocation density in the matrix originating from the interface between graphite and matrix.

The short crack growth behavior in NCI was studied by Germann et al. [39] by SEM, revealing that these cracks originate at voids formed after debonding of graphite from the matrix. Also high-

resolution synchrotron X-ray tomography [123] showed that short cracks start at casting defects and graphite nodules, but most of them arrest before initiating a macroscopic fatigue crack. Recently, Fischer et al. [37] investigated the VHCF behavior of NCI by μCT scanning and image correlation. Thereby they were able to reconstruct the strain localization during VHCF loading and so the origin of macroscopic fracture could be clearly identified, what is not always possible by SEM.

2.4.3 Fatigue crack growth

The growth of macroscopic cracks by fatigue in NCI is strongly influenced by the spatial distribution of the graphite particles, which debond from the metallic matrix when the fatigue crack approaches there. Between the particles the crack grows transgranularly resulting in fatigue striations on the fracture surface. Studies with synchrotron X-ray tomography revealed that there is a non-uniform closure process along the crack front leading to inhomogeneous arrest and growth, resp., of parts of the crack front [72, 73].

Cavallini et al. [19] investigated the influence of the matrix material (ferrite, pearlite and bainite) on fatigue crack growth by SEM. They found that the debonding of the graphite particles mainly influences the crack closure process, whereby a more pronounced debonding results in a lower crack growth rate. NCI with pearlitic matrix shows an additional secondary closure mechanism caused by shielding of the ferritic islands within the pearlite due to their different mechanical properties. It should be noted that there is only an influence of the microstructure on the fatigue crack propagation rate under high stress ratios.

Iacoviello et al. [59] found that the graphite debonding is not the main failure mechanism during fatigue crack growth. There are additional damaging micromechanisms (e.g. the so-called *onion-like* mechanism) acting in the graphite particle, which seem to be more evident. Additionally, in pearlitic NCI damage initiates in the graphite particles in form of secondary microcracks formed already in the matrix material under loading in the elastic range.

Regarding variable amplitude loading it was found by Hübner et al. [50] that the occurring effects after overloads differ from those in steel: In ferritic NCI there is a pronounced crack growth acceleration when an overload of intermediate to high load level is applied. On the microstructural level debonded graphite particles and secondary cracks were found in front of the crack tip. Later, Zybell et al. [131] identified these effects as the start of ductile crack initiation, which are accompanied by the evolution of a large plastic zone, crack branching, and early stages of ductile crack growth. The same microstructural characteristics were found in pearlitic NCI, where multiple overloads resulted in a much more tortuous crack path than that of a normal fatigue crack [60].

3 Classification of models

The modeling approaches used in literature so far can be classified according to several criteria. The first important criterion is the damage mechanism to be addressed: ductile failure (Figure 6a), cleavage (Figure 6c) and fatigue or interactions thereof. Regarding ductile failure it can furthermore be distinguished whether only the primary voids originated from debonded graphite particles are considered or whether the typically much smaller secondary voids nucleating from inclusions (Figure 6d) are incorporated, too. Regarding modeling, the ductile mechanism by growth and coalescence of primary voids is by far the mostly investigated mechanism. From this point of view all mechanisms of degradation of the metallic matrix around the primary voids, i.e. nucleation and growth of secondary voids, cleavage and fatigue, may be termed as secondary damage mechanisms.

Closely related to the damage mechanisms is the classification regarding loading conditions, which can be subdivided into time history and spatial distribution. Regarding time history the main types are monotonous loading or cyclic loading, the latter typically for addressing fatigue. One may distinguish further according to the rate of loading between (quasi-)static and dynamic conditions, i.e. whether

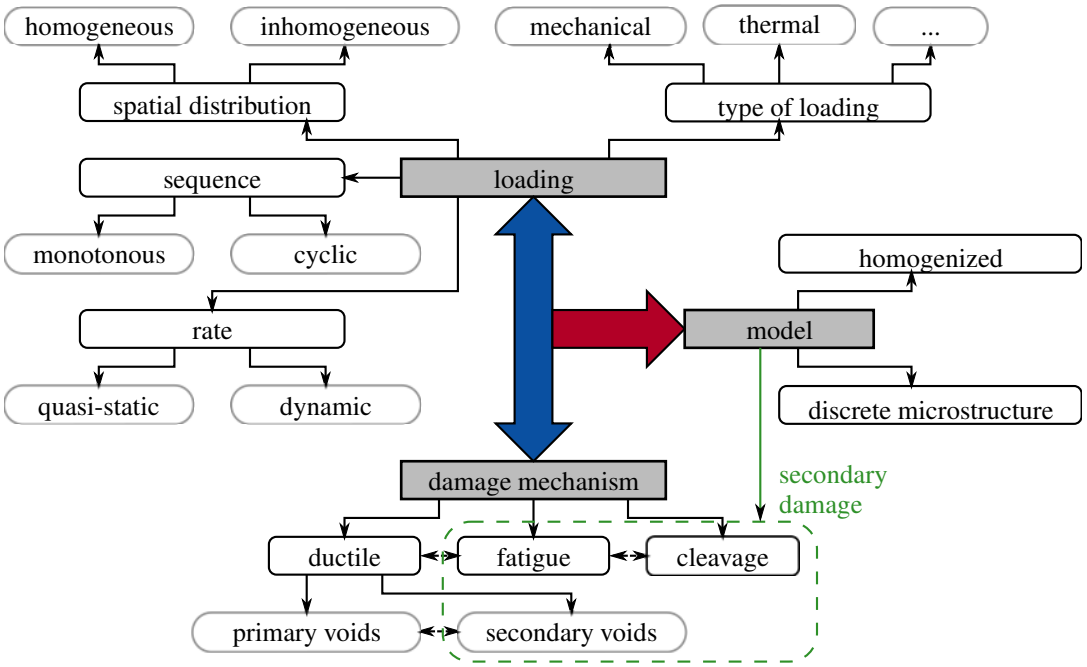

Figure 7: Classification of loading, damage mechanisms and models

inertia has to be incorporated or not. The rate of loading determines also whether strain rate sensitivity of the material is relevant and whether simplifying assumptions like isothermal or adiabatic conditions are feasible. From the many types of loading (mechanical, thermal, chemical, electrical, etc.) that may arise in real structures the present paper mainly focuses on mechanical loadings.

The second important issue of the characterization of the loading is its spatial distribution. Here the main question is whether the characteristic length scales of the macroscopic stress fields and of the microstructure are comparable or not. If the change of the macroscopic fields over characteristic length scales of the microstructure is negligible, then the loading is homogeneous with respect to a characteristic section of the microstructure and scale separation approaches (homogenization techniques, cell models) can be applied. In contrast, if the relevant length scales of the microstructure compare to the characteristic length scales of the macroscopic fields, e.g. at crack tips, sharp notches or after localization, then the loading of a characteristic section of the microstructure is inhomogeneous and the interaction of the length scales must be incorporated. This can be achieved by resolving the microstructure discretely in respective regions. Of course, in general the relevant length scales depend on the active damage mechanisms and thus also on loading conditions (rate, sequence, etc.). In NCI the heterogeneous microstructure formed by the graphite particles constitutes the relevant scale for several damage mechanisms. The main criteria for classification of damage mechanisms, loading and models and their interactions are shown schematically in Figure 7.

In contrast to experiments, the question, whether the loading is homogeneous or inhomogeneous with respect to characteristic dimensions of the microstructure, is very important for the modeling strategy. The reason is that the choice of applicable modeling techniques depends strongly on the answer of this question. That is why within the present paper this distinction is chosen as primary criterion for the classification of models used in literature.

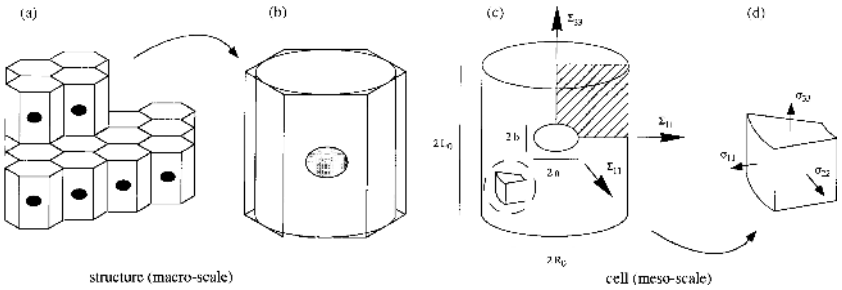

Figure 8: Concept of cell models (from [109])

4 Homogeneous stress states

4.1 Cell models

4.1.1 Concept and analytical solutions

If the macroscopic fields do not change significantly over distances comparable to the spacing of the graphite particles, it is sufficient to consider one representative cell of the material microstructure within a homogenization concept. Mostly, an idealized configuration is chosen with a spherical or ellipsoidal graphite particle arranged regularly within a spherical, cylindrical or polyhedral cell as sketched in Figure 8. For the homogenization, the macroscopic values of stresses $\boldsymbol{\Sigma}$ or rates of deformation $\boldsymbol{D}$ are prescribed to the cell model of volume V via suitable static, kinematic or periodic boundary conditions. The respective other (so-called "conjugate") quantity then derives from the requirement that the macroscopic work of deformation shall be equal to the corresponding microscopic average, the so-called *Hill-Mandel condition*:

$$\boldsymbol{\Sigma} : \boldsymbol{D} = \frac{1}{V} \int_V \boldsymbol{\sigma} : \boldsymbol{d} \, \mathrm{d}V. \tag{4}$$

Therein, σ and $\boldsymbol{d}$ refer to the tensors of stress and rate of deformation at the microscale, respectively. In the majority of cell models used in literature kinematic boundary conditions are employed (since they lead to a rigorous upper bound solution). A few studies focusing on shear-dominated loading states employ periodic boundary conditions. For details we refer to a review article by Benzerga and Leblond [10]. In cell models the loading state is often characterized by the stress triaxiality T which corresponds to the ratio of hydrostatic and equivalent Mises parts of the macroscopic stress tensor $\boldsymbol{\Sigma}$.

Furthermore, cell models that have used for NCI in the literature so far differ in the geometry of the cell, in the representation of the graphite, in the constitutive law employed for the metallic matrix and in the loading history (static or cyclic, see Section 3). In most of the studies a regular cell with spherical, cylindrical or cubic shape is investigated. Cubic cells can be arranged to fill a room completely at the cost that the global response is in general anisotropic, a drawback that is seldom mentioned. In contrast, spherical or cylindrical cells can fill a given room only approximately (Figure 8). However, with corresponding constitutive laws for the constituents, spherical cells lead to a macroscopically isotropic behavior which is typically expected for a material like NCI. In the literature, spherical cells were almost exclusively used if the microscopic boundary value problem was to be solved analytically. Aiming at a closed-form solution, such approaches have to limit the complexity of the representation of matrix and graphite, i.e. typically an ideal-rigid plastic behavior of the matrix is assumed and the particle is modeled as a void. Surely, the most famous model of this limit-load type was formulated by Gurson [46]. Numerous extensions of Gurson's homogenization approach have been proposed in the literature taking into account e.g. void-shape effects or secondary voids.

4.1.2 Numerical approaches

However, if the behavior on the microscale shall be modeled in more detail, either for improved quantitative predictions or for qualitative understanding of mechanisms like void coalescence, then analytical solutions are not available anymore and numerical methods are necessary. Mostly, the finite element method is employed. In such numerical models typically cubic cells or cylindrical cells (implemented by means of axisymmetric elements) are used due to the periodicity and since especially in large displacement analyses, the implementation of the boundary conditions is easier than with spherical cells. In this context the pioneering work of Tvergaard and co-workers has to be mentioned [67, 114, 115] which improved considerably the understanding of the ductile failure mechanism in metals. Based on the results of the cell models, heuristic modifications of the Gurson model were proposed by Tvergaard and Needleman [114, 119], namely the parameters q_i and the effective void volume fraction f^*. This modified model is today well-established and known as GTN-model. Note that in cell models, independent of whether treated by numerical or analytical methods, in general the size of the cell, which is related to the graphite distance λ drops out due to division by the volume V in Eq. (4). Thus, in such models the resulting macroscopic behavior can only depend on λ if approaches for secondary mechanisms are applied on the microscale incorporating internal lengths (e.g. non-local or gradient approaches or cohesive zone models). However, even in these cases the resulting influence of λ is rather indirect over relations that then the macroscopic values e.g. of strain to failure or yield stress may depend on the ratio of the internal length and λ.

4.2 Cell models for nodular cast iron

4.2.1 Modeling graphite as primary void

About ten years after the pioneering studies of Tvergaard and Needleman, cell models were applied to NCI for the first time [18, 27, 31, 69, 109, 130]. In the first studies the graphite particles were modeled as a priori existing voids with a volume fraction of $f_0 \approx 10\%$. Thereby, it is essential to represent the elastic-plastic properties of the matrix material adequately. In [18, 69, 109] the yield curve of the matrix was extracted from tensile tests on "ferritic bulk material which has the same mechanical properties as the matrix material in cast iron". A similar approach was used by Dong et al. [31] and verified by microhardness tests on NCI. Focussing on the initial plastification, Dahlberg [27] assumed (almost) ideal plastic behavior of the matrix. [130] do not provide sources for their assumed yield curve of the matrix.

Qualitatively, these cell model studies on NCI comply with the main findings of preliminary studies [67, 114, 115] with much lower void volume fractions, especially regarding the influence of stress triaxiality on void growth and evolution of void shape, Figure 9. These simulations were also used quantitatively to calibrate the heuristic parameters of the GTN-model for this material. It was found that for the large void volume fractions, which are representative for the graphite in NCI, the parameters q_1 and q_2 of the GTN-model have to be chosen lower than the values $q_1 = 1.5$ and $q_2 = 1.0$ proposed by Tvergaard for lower void volume fractions, namely in the range $q_1 = 1.1 \ldots 1.3$ and $q_2 = 0.7 \ldots 1.0$ [18, 69]. It turned out that the particular spatial arrangement of the voids and the shape of the void and the cell have only little influence on the initial yield point and the following hardening behavior. However, spatial arrangement and shape do have a moderate effect on the instant of transition to the void coalescence stage [69, 109, 130]. For instance it is found that oblate voids whose long axis are aligned normal to the main loading direction lead to an earlier void coalescence [18], the reason why cast iron with lamellar graphite has considerably lower strains to failure than NCI. For low stress triaxialities there is also a moderate effect of the third invariant of the stress deviator (expressed typically by the Lode parameter) on the strain to failure [132].

Fritzen et al. [38] investigated a cell with a large number of stochastically arranged spherical voids and compared it to the behavior of the classical simple model of a cell with only a single void, i.e. a periodic arrangement. Although not aiming explicitly at this material, they used void volume fractions

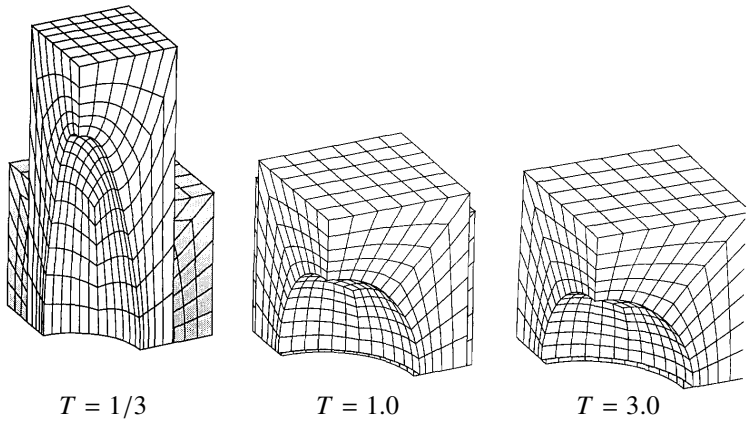

Figure 9: Effect of stress triaxiality T (from [69])

of 10%, which are representative for the debonded graphite in NCI. In coincidence with the studies cited above it is found that the difference of the predicted initial yield stress between the different realizations is relatively low. In contrast, Nicoletto et al. [87] performed cell model simulations with two voids of different size to investigate the effect of deviations from periodic arrangements. They report that the macroscopic yield stress decreases with increasing difference of size of both voids. Presumably, this finding can be attributed to the employed series connection of both elementary unit cells.

4.2.2 Modeling of graphite particles

Addressing the question whether the graphite can be indeed modeled as void, Brocks and Steglich [18, 109] performed for comparison cell model simulations with the graphite particle represented as a rigid, unbonded particle. For low triaxialities $T = 1/3$ (i.e. uniform macroscopic tension) they observed hardly any effect in the initial regime of deformation. However, concerning the initiation of void coalescence the explicit modeling of the graphite particle has a considerable effect, see Figure 10. The cell model with graphite particle predicts an earlier coalescence since the graphite hinders the lateral contraction thus favoring necking of the metallic matrix, compare Figure 4. Modeling the graphite as rigid particle is of course a strict assumption so that this model surely overestimates the effect of the graphite. Dong et al. [31] compared simulations with a void and those with a perfectly bonded elastic graphite particle. As could be expected from the observed early debonding of graphite particles reported in Section 2, the model with void gives a better agreement to experimental results. Collini and Nicoletto [23] investigated cell models with and without unbonded elastic graphite particles. Hardly any difference between the results of both simulations is observed. However, these authors simulated only the initial regime of yielding but not the coalescence stage. Bonora and Ruggiero [17] modeled the graphite particles also as unbonded and elastic but incorporated the cooling from solidification to room temperature. The different thermal shrinkage of graphite and matrix during cooling leads to compressive stresses at the graphite matrix interface at room temperature. The authors performed a systematic parameter study on the effect of the elastic properties of the graphite which are, by the way, not trivial to determine. Finally, their model allowed adequate predictions of the material behavior around the yield point and with respect to the tension-compression asymmetry of NCI. Focussing on the regime of initial yielding, the results of Bonora and Ruggiero [17] show that above strains of about 0.5 % and for positive stress triaxialities the graphite particles can be modeled as voids. Aiming at machining simulations, Chuzhoy et al. [22] incorporated also the inelastic properties of the graphite.

A number of recent papers focused on ductile failure under low stress triaxialities or even pure shearing by means of cell model simulations [88, 117]. These studies investigate the mechanism in principle, thus

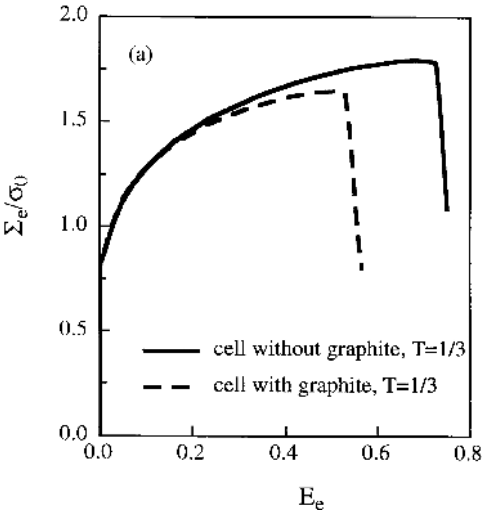

Figure 10: Effect of incorporating the graphite as rigid particle (from [109])

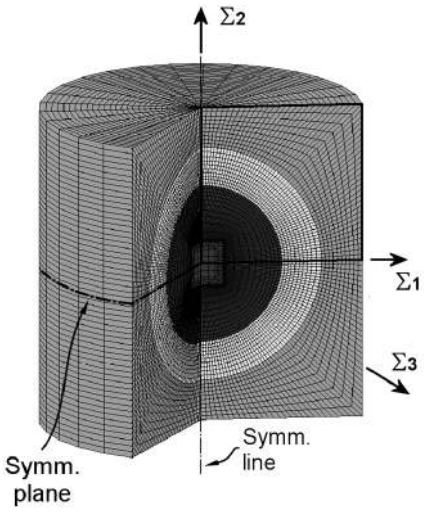

Figure 11: Cell model with bull's eye structure (from [23])

using voids with a volume fraction only up to 5%. It is found that especially under pure shearing the voids shut thus forming microcracks. Regarding NCI it is clear that the graphite particles will prevent the closure and will thus affect this mechanism. In this context also inelastic deformation properties of the graphite have to be taken into account.

4.2.3 Microstructure of the matrix

Another aspect that has been investigated is the microstructure of the metallic matrix, especially for ferritic-pearlitic cast irons. For this purpose the bull's eye structure (Figure 1b) was resolved in cell model simulations [22, 23, 64, 86, 87] as shown in Figure 11. Chuzhoy et al. [22] extracted the elastic-plastic properties of ferrite and pearlite individually from heats resembling both constituents. In contrast, Collini and Nicoletto [23, 86, 87] performed an inverse parameter identification based on some ad-hoc assumptions. With these models, Kobayashi and Toda [64] focused on the initiation of microcracks, whereas Collini and Nicoletto [23] could predict correctly the effect of the ferrite content on the macroscopic yield stress. The predictions of the macroscopic yield curve were improved in [86, 87] by considering deviations from the idealized single unit cell model. Metzger and Seifert [80] simulated the yielding of lamellar cast irons assuming a single yield curve for the pearlite-ferrite composite of the matrix. This single composite yield curve was determined by an inverse parameter identification.

Furthermore, fractographic investigations of NCI do not exhibit only the large dimples originating from the graphite particles (Figure 6a) but in-between these dimples, smaller ones are found stemming from a second population of void nucleating particles in the matrix like carbides, Figure 6d. This finding implies the question for the relevance of these secondary voids to the macroscopic behavior of the material. Typically, the secondary voids are much smaller than the graphite particles. That is why already in some of the first papers [18, 69] on cell models for NCI, comparative studies were performed modeling the matrix material in a homogenized way by the GTN-model. Brocks et al. [18] used an initially present secondary porosity of 0.04% "which did not show any effect". In contrast, Kuna and Sun [69] assumed a nucleable secondary porosity of 0.8% which lead indeed to an earlier initiation of the coalescence of the primary voids originating from the graphite particles. The problem with the GTN-model and any other constitutive law formulated within the framework of simple materials is that the boundary value problem becomes ill-posed in the softening regime leading to a pathological mesh dependency of the results in FE simulations.

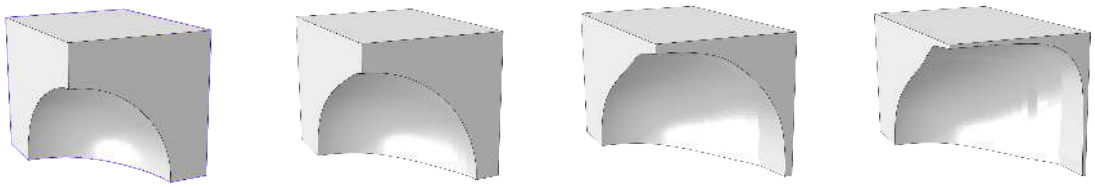

(a) $\lambda/l_2 = 20$ (b) $\lambda/l_2 = 5$ (c) $\lambda/l_2 = 2$ (d) no secondary voids

Figure 12: Deformed configurations of the unit cells at final failure for various internal lengths showing different remaining ligament widths (from [132])

In order to overcome this problem in [132] an implicit gradient-enriched nonlocal GTN model was used for the matrix thus also incorporating the mean distance l_2 of secondary voids. It is found that the ratio of l_2 to the distance of primary voids λ influences especially the coalescence stage: the larger λ is compared to l_2, the earlier the primary voids coalesce. This effect was found to correspond to experimental results of NCI. Correspondingly, λ/l_2 affects the remanent ligament width at final failure as shown in Figure 12. For a matrix without secondary voids (Figure 12d), the macroscopic softening is attributed only to the geometric softening of the ligaments during the plastic collapse (in this context known also as *internal necking*).

Bonora and Ruggiero [17] employed heuristically an effective stress-type continuum damage model to account for the "ductile damage" of the matrix. Chuzhoy et al. [22] utilized a Cocks-Ashby model to implement the material degradation both of metallic matrix and of the graphite. Recently, Dahlberg et al. [26] used the Guo-Faleskog-Shih model [45] to reproduce the macroscopically observed tension-compression asymmetry. This model has been derived analytically similar to Gurson's one by a limit load analysis of a spherical cell but using a dilatational Drucker-Prager matrix instead of a Mises matrix. The Drucker-Prager law of the matrix is not symmetric with respect to tension and compression. In contrast, Bonora and Ruggiero [17] explained the macroscopic tension-compression asymmetry with the contact between matrix and graphite particle as mentioned above. Apparently, the reasons for the tension-compression asymmetry require further research.

4.3 Cyclic loading and fatigue

Cell model simulations with spherical voids under cyclic loading were first performed by Gilles et al. [41] demonstrating that, as can be imagined, the behavior does not depend only on the monotonous yield curve but on the relation between kinematic and isotropic hardening of the matrix. This study and further ones [e.g. 29, 99, 110] showed an increase of the void volume within each cycle, the so-called *ratcheting* effect. This effect was shown to be attributed to the formation of elastic zones after load reversal. The effect of kinematic and isotropic hardening was also investigated for larger void volume fractions [106]. Seifert and Riedel [105] proposed a heuristic extension of the Gurson model to capture thermomechanical fatigue (TMF) of cast irons.

The results of Gilles et al. [41] also indicated an accelerated void growth under tension after a compression preload compared to monotonous tension without preload. In NCI, under compression the matrix interacts with the graphite particle. This effect was investigated by Rabold and Kuna [97] by comparing the predictions of cell models with a void and those with a rigid unbonded graphite particle for a stress ratio of $R = -1$. The results show that the model with void predicts a stronger ratcheting than the one with rigid particle, see Figure 13. This effect depends surely on the stress ratio R as well as on the particular modeling of the graphite. Chuzhoy et al. [22] applied a more sophisticated model for the graphite. However, these authors simulated only a single tension-compression cycle as

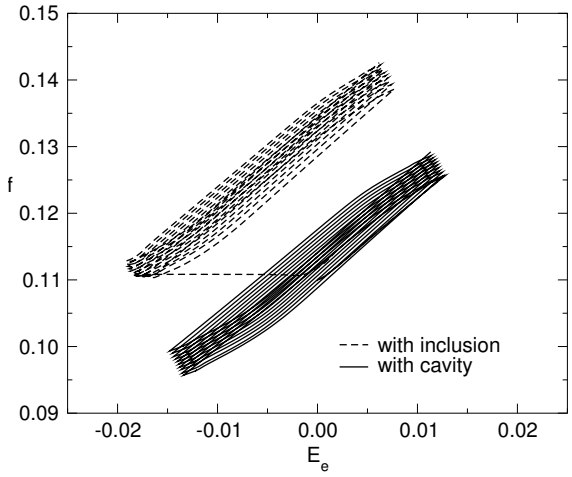

Figure 13: Effect of representation of graphite on ratcheting (from [97])

this is relevant for their machining simulations. Fatigue growth of microcracks emanating from graphite particles was studied applying linear-elastic fracture mechanics by Dahlberg [27].

5 Inhomogeneous stress states

5.1 Fracture simulations with discrete primary voids

5.1.1 Ductile fracture

For the ductile crack propagation in NCI, the mean distance λ of graphite particles was recognized as relevant microstructural length scale since experiments show a strong relation between λ and fracture toughness, compare Figure 2. A straight forward way to investigate the relation between microstructure and ductile fracture is to resolve the microstructure in the fracture process zone discretely. There, strong gradients appear which can be accounted for adequately by a discrete representation of the microstructure. Under the large triaxiality and straining in the process zone, at least under monotonous mode-I loading to be considered in the following, the graphite particles can be modeled as a priori existent voids as discussed in Section 4. In sufficient distance to the process zone, the gradients of the field quantities become irrelevant such that the material behavior there can be described in a homogenized way as shown schematically in Figure 14. Mostly, models of this type are applied to ideal small scale yielding conditions so that the far-field is uniquely defined by the stress intensity factor K_{I}. This limit case excludes possible effects of the geometry of a particular specimen (constraint effects) — a big advantage of numerical simulations in the light of the large effort to perform small-scale yielding fracture experiments for ductile metals. Of course such models with discrete microstructure can be applied also to specimens of finite size if desired.

The first models with resolved microstructure in form of a single circular discrete void were presented 30 years ago [1, 2]. But it took almost 20 further years until Tvergaard and Hutchinson [118] considered a whole set of voids in front of the crack tip and discovered that the mechanism of ductile crack propagation depends on the initial void volume fraction f_0. For low void volume fractions the voids in the crack plane grow one after another (Figure 15a, *void-by-void mechanism*), whereas for larger void volume fractions the currently active process zone encompasses several voids and shifts continuously along the crack plane (Figure 15b), the so-called *multiple void mechanism*. Tvergaard and Hutchinson [118] pointed also out that for dimensional reasons the fracture toughness (in terms of the J-integral)

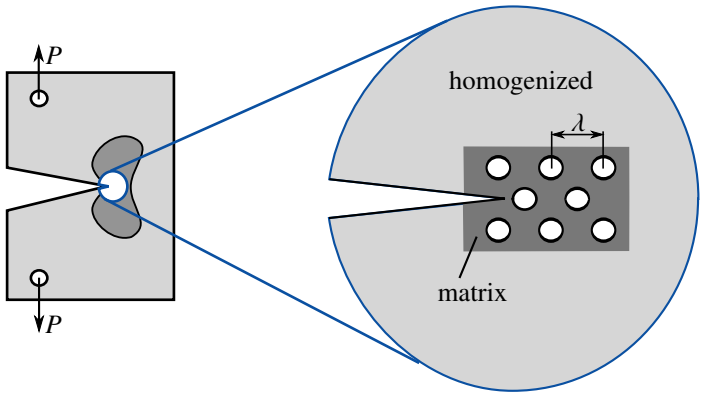

Figure 14: Model with discretely resolved voids in the process zone

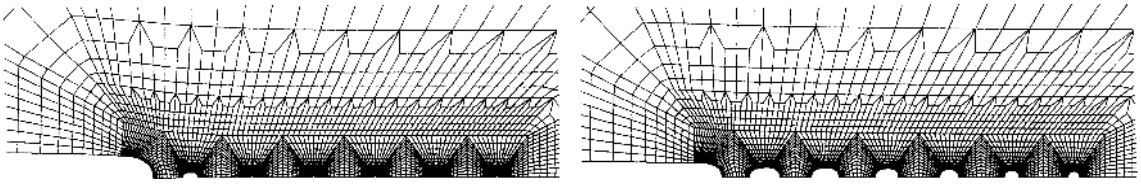

(a) (b)

Figure 15: Influence of void volume fraction f_0 on ductile mode of crack propagation: (a) void-by-void mechanism of void growth for low $f_0 = 0.00087$, (b) mutiple void mechanism for higher $f_0 = 0.014$ (from [118])

predicted by such a model must have the structure

$$\frac{J_c}{\lambda\sigma_0} = \text{function}\left(f_0, \frac{\sigma_0}{E}, N\right) \tag{5}$$

if the constitutive law of the matrix material does not contain a further length scale. The latter condition is fulfilled for all laws formulated within the framework of simple materials like Mises plasticity or GTN-model. In Eq. (5), σ_0 and E denote the yield stress and Young's modulus, respectively, and N is the hardening exponent.

According to the mentioned results of [118], NCI with its early debonding graphite particles of a relatively large volume fraction should exhibit a multiple void mechanism of ductile crack propagation. The simultaneous growth of several voids in front of the initial crack tip is also observed in experiments, see Figure 5b. However, for this mechanism the model of Tvergaard and Hutchinson [118] predicts a normalized fracture toughness of $J_c/(\sigma_0\lambda) \approx 0.5$. For a ferritic NCI with $\sigma_0 = 270\,\text{MPa}$ and $\lambda = 50\,\mu\text{m}$ this would correspond to a fracture toughness of $J_c \approx 6\,\text{N/mm}$. However, Figure 2 shows that measured values are at least two times higher.

An extension towards a 3D model with spherical voids [62] increased the predicted normalized fracture toughness $J_c/(\sigma_0\lambda)$ for the multiple void mechanism only moderately. Simultaneously, a model with discrete voids at the crack tip was applied the first time explicitly to NCI by Dahlberg [28], though not aiming at ductile failure but at the crack closure effect during fatigue. However, apparently the research groups [62, 118] and [28] did not take note of each other.

Reasons why the models of [62, 118] strongly underestimate fracture toughness and crack growth resistance of NCI were identified recently. In [62, 118] the homogenized behavior outside the discrete void region was modeled by Mises plasticity with identical parameters of the matrix material. In [57] such simulations were compared to simulations allowing also for void growth around the process zone. The void growth around the process zone, which is observed in experiments as well as discussed in Section 2.4.1, was incorporated by resolving several layers of discrete voids and by embedding this discrete zone in a homogenized region modeled by the GTN-model. A comparison of the crack growth resistance curves predicted by this consistent model with the above-mentioned models of a single layer of voids embedded in Mises material shows that the consistent model predicts an about twice as high crack growth resistance. The reason of this behavior is that the void growth in the plastic zone shields the process zone from hydrostatic stresses thus retarding the void growth in the process zone. Of course the shielding effect is the stronger, the higher the void volume fraction is. Thus, for NCI it plays an important role.

In all of the studies on fracture simulations cited until now in this section, a hardening exponent of $N = 0.1$ and a relative yield stress $\sigma_0/E = 0.003$ of the matrix material were assumed, both values seen as representative for intermediate strength steels and light-weight alloys. However, systematic studies on the effect of these parameters [51, 58] showed that both N and the ratio σ_0/E have a very strong influence on the predicted fracture toughness and on the tearing behavior: the higher N is, the higher are the normalized fracture toughness $J_c/(\sigma_0\lambda)$ and the slope of the crack growth resistance curve.

The reason for the strong effect especially of the hardening is that with sufficiently ductile matrix material, the *internal necking* of the microligaments between the voids (or graphite particles, respectively) is the dominating mechanism: after certain straining the geometric softening due to lateral contraction of the microligaments cannot be compensated anymore by the hardening of the matrix material. In cell models this limit load is typically defined as the initiation of void coalescence stage. In fracture simulations with discrete microstructure, at this point the active process zone moves forward even without material separation which corresponds effectively to crack growth. The competition between strain hardening and geometric softening explains the strong influence of the elastic-plastic properties on the ductile R-curve. In [58] the hardening exponent of ferritic matrix material was extracted from experiments as $N = 0.20$, i.e. considerable larger than assumed before. R-curves simulated with a 3D model with regularly arranged spherical voids, incorporating the shielding effect and using realistic elastic-plastic properties of the matrix are plotted in Figure 16. The comparison with corresponding

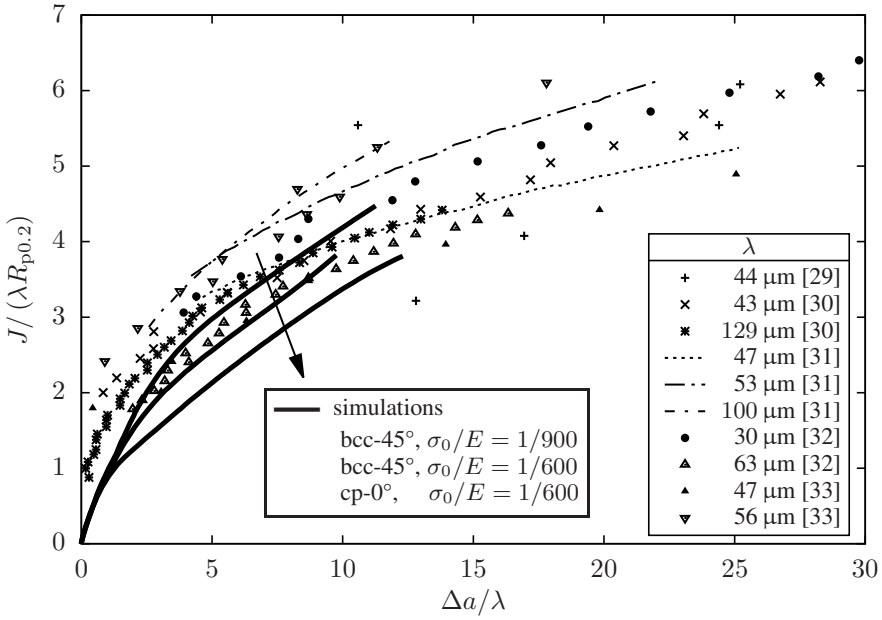

Figure 16: Predicted R-curves from simulations with discrete voids in comparison to experimental data (from [58], for references in legend c.f. [58]; $R_{p0.2}$: 0.2% offset yield stress with $R_{p0.2} = 250\,\text{MPa} \ldots 315\,\text{MPa}$)

experimental data for ferritic NCIs EN-GJS-400 shows that the model allows realistic predictions for a wide range of mean distances λ of graphite particles just from the geometry of the microstructure (f_0 and λ) and elastic-plastic properties of the matrix (σ_0, E, N). Note that Figure 16 contains simulation results for two basic arrangements of the discrete voids, cubic primitive (cp) and body-centered cubic (bcc). The curves deviate moderately, similarly as the void volume fractions at coalescence in cell models depend on the particular geometry. Figure 16 shows that the cp arrangement underestimates the R-curves. This is plausible since in this case, a layer of voids with shortest distances among each other is favorably located directly in the crack plane. In the bcc arrangement there is no such favorable plane of least crack growth resistance. Thus, it is proposed to employ the bcc arrangement for fracture simulations of NCI with discretely resolved microstructure if the stochastic distribution of the graphite particles shall not be addressed explicitly. Due to the multiple void mechanism, the effect of the displaced location of single graphite particles on the ductile failure is surely limited.

The simulated R-curves in Figure 16 were predicted with a model, which incorporates only internal necking of the microligaments but no material separation (e.g. due to cleavage or secondary voids, compare Figure 6). This fact raises the suspicion that internal necking is the main mechanisms for ductile failure of ferritic NCI at room temperature. Apparently, due to the multiple-void mechanism the actual material separation is of minor importance as long as it happens late enough after the plastic limit load of the individual microligaments is exceeded. This finding explains the difficulties in defining suitable measures of crack growth Δa and thus of fracture initiation, both in experiments and in simulations. It even implies the question for the usefulness of the concept of a "physical" fracture initiation for this material at all.

Anyway, if a more or less exactly determinable point of the crack growth resistance curves in Figure 16 is defined as fracture initiation, then Eq. (5) holds[2], that means J_c is proportional to the graphite distance λ. In contrast, empirical relations as in Figure 2 predict a finite J_c for $\lambda = 0$. We think that

[2]Eq. (5) does *not* hold if additional length scales are introduced for the fracture initiation, e.g. if the fracture toughness is defined as $J(\Delta a = 0.2\,\text{mm})$.

this discrepancy has several reasons: Firstly the additional normalization of J_c with respect to the yield stress σ_0 (or $R_{p0.2}$, resp.) in Eq. (5) and Figure 16 eliminates the Hall-Petch effect. This effect is surely relevant in absolute graphs like Figure 2 since grain size and λ are proportionally correlated as many micrographical analyses have shown. Secondly, the uncertainties in measuring Δa in the range of one or two λ, where the simulated curves in Figure 16 exhibit the first deviation from the blunting line, and the associated problem of an exact determination of J_c should not be underestimated. And thirdly, for fine dispersed NCIs with $\lambda \lesssim 20\,\mu m$ further length scales associated with secondary mechanism (secondary voids, cleavage) may become relevant.

In all models used to simulate ductile fracture of NCI with resolved microstructure in the process zone, the graphite is modeled as voids. Results from cell models in Section 4 showed that this is justified as long as there are positive hydrostatic stresses and at least moderate plastic deformations. Both is definitely the case in the fracture process zone. However, results cited above from simulations of crack growth showed that even the void growth outside the process zone is important for the shielding mechanism. But somewhere in this region there must be the transition between bonded and debonded graphite particles. Simulations incorporating the graphite particles and the thermal eigenstrains as in cell models [17] can shed light on the question whether the debonding affects the shielding effect. A second effect that is not considered in the cited studies is the strain rate dependence of the yield stress. The available models with rate-independent plasticity of the matrix predict that already for far-field loading rates $\dot{K}_I$ which are typically considered as "static", local strain rates evolve in the microligaments which would lead in macroscopic tensile tests to increased yield stresses. An increased yield stress of the matrix would, for ideal ductile failure, imply a higher crack growth resistance. On the other hand, fast strain rates on such small lengths of some ten microns would correspond to quasi-adiabatic conditions and the heating associated with the large local plastic deformations would lower the yield stress. Anyhow, those models neglecting debonding, strain rate sensitivity and adiabatic softening allow already reasonable predictions as demonstrated by the good agreement with experiments in Figure 16. This finding raises the suspicion that these effects cancel out each other at least under macroscopically quasi-static loading conditions. Nevertheless, it will be an important issue for future research to incorporate and quantify these effects since the "weights" between the effects can be shifted, e.g. under dynamic loading or if secondary damage mechanisms become dominant.

5.1.2 Secondary voids, cleavage and fatigue

In addition to the debonding of graphite particles and the growth of the thereby created primary voids, secondary damage mechanisms are observed on the microscale. This is the formation of smaller secondary voids as well as cleavage and fatigue of the metallic matrix, appearing in the ligaments between primary voids.

Models with discretely resolved primary microstructure in the process zone (Figure 14), i.e. discrete graphite particles or voids, are appealing for investigating the effect of secondary damage mechanisms since the complex interactions are caught directly. The idea to model the secondary mechanisms in a homogenized way for the matrix material between the discrete primary voids in the process zone does suggest itself. That is why such models were presented in the 1980s at the same time with the first models containing a single discrete void in the process zone. So Aoki et al. [1] and Aravas and McMeeking [3] employed the GTN model to account for the growth of secondary voids (the same way as in cell models, Section 4.2.3) and investigated their effect on ductile fracture initiation. Figure 17 shows the obtained distribution of the volume fraction of secondary voids between the blunted crack tip on the left-hand side and the primary void ("hole"). The problem when using the classical GTN model is that in the softening regime the results exhibit a pathological mesh sensitivity as will be explained in detail in Section 5.2. In order to overcome this problem nonlocal [55] and micromorphic extensions [112] of classical ductile damage models (GTN and Cocks-Ashby, resp.) were used for the matrix material instead. In addition, such approaches with intrinsic length scale allow to study the effect of the size of secondary voids. In [55] it is found that for small primary void volume fractions the size of the

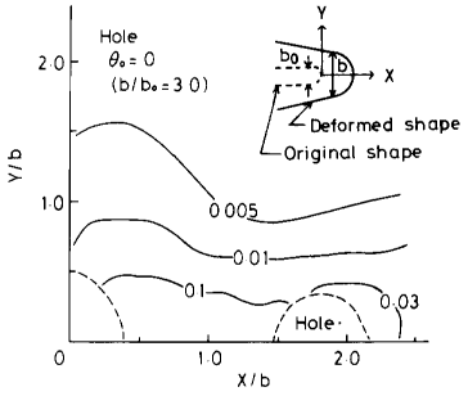

Figure 17: Secondary void volume fraction between the primary void and blunted crack tip (from [1])

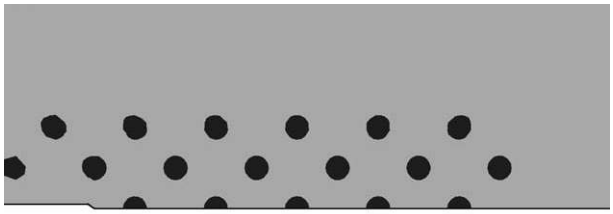

Figure 18: Process zone model with islands of nucleable porosity (from [121])

secondary voids has a strong effect. In contrast, for larger primary void volume fractions this influence is considerably weaker due to the prevailing multiple-void mechanism.

In several papers Needleman and Tvergaard (e.g. in [84, 85, 121]) employed models with partly smeared microstructure in the process zone. In particular, they used a (modified) GTN model in the whole domain for the secondary voids but modeled the microstructure as (circular or spherical) "islands" of higher nucleable porosity for the primary microstructure as shown in Figure 18. For the relatively high volume fraction of islands, e.g. in [84], their simulations exhibit a smooth transition from crack tip blunting to void growth in agreement with the behavior of NCI observed in experiments and in simulations with discrete voids. The discrete-islands representation allows a computationally efficient simulation of relative large regions with discrete microstructure. However, since based on the local GTN-model the results suffer also from the pathological mesh dependency.

Fatigue is another mechanism of degradation of the metallic matrix that was investigated by means of models with discretely resolved microstructure. Dahlberg [28] applied a model with several discrete voids to study fatigue fracture initiation in NCI. For this purpose he applied a post-processing criterion of Manson-Coffin type to the local plastic strains between the voids. Collini and Pirondi [24] simulated the fatigue crack growth initiating at a discretely resolved mesoscale casting defect by means of classical fracture mechanics with a Paris law.

In a similar way, Petti and Dodds [94] evaluated possible cleavage initiation in the DBT regime by applying a Beremin post-processing criterion to the local fields between the discrete voids. Needleman and Tvergaard [85, 120] extended their models with islands of nucleable porosity by a node-release technique with a Ritchie-Knott-Rice criterion to simulate crack propagation by cleavage ("cleavage grains"). In [54, 56] material degradation by cleavage is additionally incorporated by means of a cohesive zone in the crack plane between the discrete voids. This approach allows to simulate crack propagation by cleavage and by the ductile mechanism equivalently. However, it is found that the 2D model in [54] with circular voids oversimplifies the competition between both mechanism which is why the 3D model

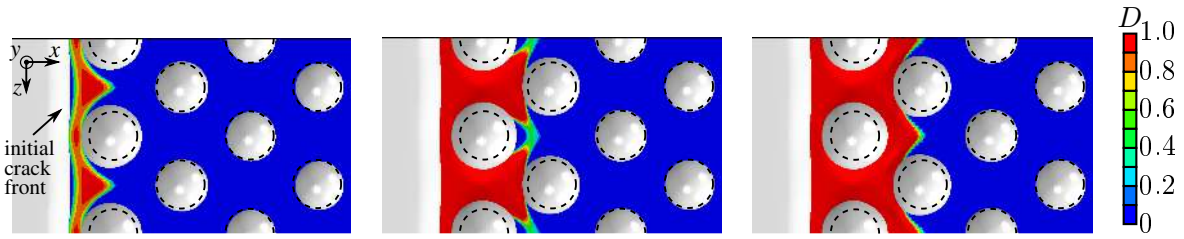

(a) $J = 1.01\,\sigma_0\lambda$ (b) $J = 1.21\,\sigma_0\lambda$ (c) $J = 1.26\,\sigma_0\lambda$

Figure 19: Evolution of cleavage material degradation D in the crack plane in competition with void growth with increasing far-field loading J (dashed: initial configuration; from [56])

with spherical voids in [56] is necessary. Figure 19 shows the predicted competition between ductile mechanism (void growth) and cleavage from the 3D models.

The results in [55, 55, 56] demonstrate that for high primary void volume fractions as representative for NCI, the predicted crack growth resistance curves are relatively insensitive to certain amounts of secondary damage, secondary void growth and cleavage resp., due to the prevailing multiple void mechanism. This explains why the experimental R-curves given in Figure 16 in normalized form lie within a relatively narrow band compared e.g. to steels which fail by a void-by-void mechanism.

5.2 Fracture simulations with homogenized models

5.2.1 Ductile fracture

Despite their physical validity, the big disadvantage of fracture models with discretely resolved microstructure in the process zone is the resulting large computational effort. At the beginning of the development in the 1980s, such models could thus be used only for a few fundamental studies but rarely for direct engineering applications. That is why for engineering structures, macroscopic material laws representing the homogenized material behavior in an adequate way were desirable also for simulations of crack propagation. The GTN-model (and its descendants) are established for describing the homogenized failure behavior of ductile metals. The problem of the GTN-model and most of its descendants is that they are formulated within the framework of simple materials (i.e. only in terms of stresses and strains). Therefore, they do not contain an intrinsic length scale that could be correlated to the relevant physical length λ. Mathematically speaking, the boundary value problem becomes ill-posed if a material point reaches the softening regime leading to a pathological mesh sensitivity of the results of corresponding FEM simulations. Although not completely consistent from a continuum mechanics point of view, an established heuristic approach to overcome this problem in simulations of ductile crack propagation is to choose a regular mesh in the ligament and to declare the edge length of the elements in the ligaments as a material parameter related to the material length λ (denoted later as "computational cell approach" [127]) as sketched in Figure 20. Later, Bernauer and Brocks [14] pointed out that the height of the elements in the ligaments is the relevant quantity. This approach was also applied to NCI in several studies [11, 18, 30, 32]. Brocks et al. [18] calibrated the GTN parameters from cell models to simulate the crack growth resistance curves for two NCIs with different graphite distances λ proofing the correlation between the element length and λ, see Figure 21. Note that in [11, 18] the complete domain was modeled by the GTN model and not only the single layer of elements as proposed by Xia and Shih [127]. Thus, the model accounts also for the void growth in the plastic zone and the associated shielding effect as described in Section 5.1.

Within the computational cell approach, the GTN model itself is able to describe the growth of the voids created from debonded graphite particles. In the literature, other macroscopic models, which

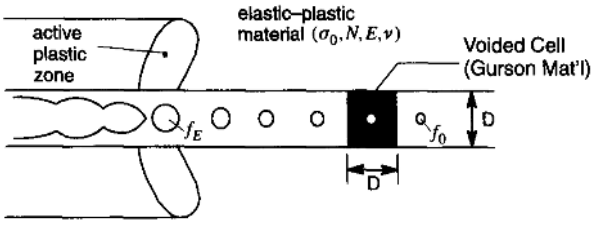

Figure 20: Computational cell model (from [127]; $D = \lambda$ in present notation)

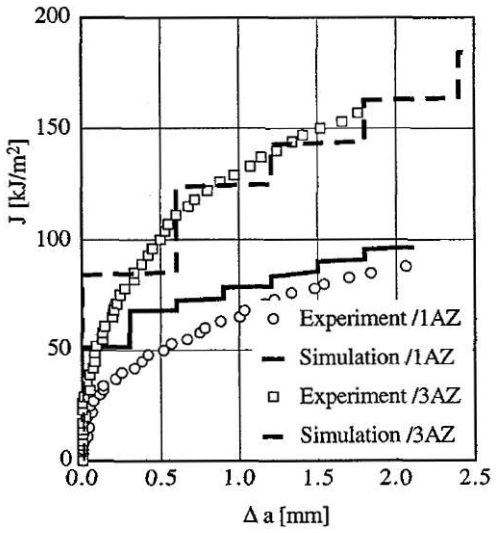

Figure 21: Predicted R-curves from simulations with computational cells in comparison to experimental data for two ferritic NCIs (1AZ with $\lambda_{\mathrm{nn}} = 51\,\mu\mathrm{m}$ and 3AZ with $\lambda_{\mathrm{nn}} = 96\,\mu\mathrm{m}$; from [18])

account for several additional details of the microscopic mechanisms, were applied to simulate ductile fracture. So Berdin et al. [11] incorporated void nucleation terms for the GTN model to address the experimentally found differences in the unloading stiffness of ferritic and ferritic-pearlitic NCIs. Pardoen and Hutchinson [93] employed a more sophisticated constitutive law consisting of the GLPD model [42] for void shape effects in combination with the Thomason model [111]. These authors investigated the effect of elastic-plastic parameters of the matrix (σ_0/E, N) and the initial void volume f_0 on the fracture initiation toughness J_c and were able to reproduce the main trends of simulations with discretely resolved microstructure. In particular, they found that the active process zone becomes wider (compared to the cell size) with increasing f_0. This widening can be interpreted as the transition from the void-by-void mechanism to the multiple void mechanism. In order to address failure of NCI under low levels of stress triaxiality, Memhard et al. [78] implemented a Johnson-Cook criterion for immediate failure of a material point for a dynamic FEM simulation with forward ("explicit") time integration.

In order to get rid of the pathological mesh dependency of the results, higher-order continuum approaches like nonlocal or strain-gradient theories are necessary, which introduce a material length consistently in their continuum mechanics formulation. Several heuristic nonlocal extensions of the GTN model were proposed in the literature and successfully used to simulate ductile crack propagation. To the authors' knowledge only in [52] such a model was used with void volume fractions f_0 that are representative for NCI. The results of [52] showed that such a nonlocal model can reproduce the effect of f_0 on the mode of crack propagation. The promising strain gradient extension of the GTN model by Gologanu et al. [42] was not applied to higher void volume fractions yet.

Another established approach to describe ductile crack propagation consistently is to "condense" the process zone into a cohesive layer embedded within non-damaging elastic-plastic materials (see e.g. [103] and references therein). To the authors' knowledge the cohesive zone approach was not applied to NCI yet either. We think that this approach is inappropriate to simulate the ductile failure of NCI since it cannot capture the relevant mechanisms for this material adequately, namely the strong interaction between process zone and void growth in the surrounding plastic zone and the associated shielding effect.

5.2.2 Secondary voids, cleavage and fatigue

In general it can be stated that it is difficult to incorporate secondary damage mechanisms in the already complex macroscopic constitutive laws, which capture the material behavior in a homogenized way. That is why only relatively few examples of this type of models can be found in literature. Regarding secondary voids, a pragmatic approach is to use a GTN computational cell model with nucleation terms and to interpret the initial void volume fraction as graphite and the nucleable porosity as secondary voids [84, 85, 121]. However, in such a model the only state variable is the total void volume fraction whose primary and secondary contributions cannot be distinguished anymore. A more detailed homogenized model for the interaction between primary and secondary voids was presented by Fabrègue and Pardoen [36], but not applied to NCI yet.

Another secondary damage mechanism that was addressed by homogenized models in the literature is cleavage. For many engineering metals, in particular ferritic steels, cleavage is the underlying mechanism of brittle failure. That is why post-processing criteria are established to evaluate cleavage initiation in such steels. The most common ones are of Ritchie-Knott-Rice type [100] or are of Beremin-type [12] based on the weakest-link assumption. NCI does not display such a direct relation between local cleavage and brittleness as discussed in Section 2.3.1 due to the multiple-void mechanism. which is why such post-processing criteria are only of limited applicability and thus not discussed here. For a review we refer to [53]. The complex interaction between cleavage and the graphite particles in NCI requires an equivalent modeling of both damage mechanisms.

For this purpose in [68, 82] Kachanov-Lemaitre effective stress type damage models for cleavage were combined with ductile damage models within a computational cell approach. Another approach that leads to a well-defined boundary value problem thus overcoming the pathological mesh sensitivity was

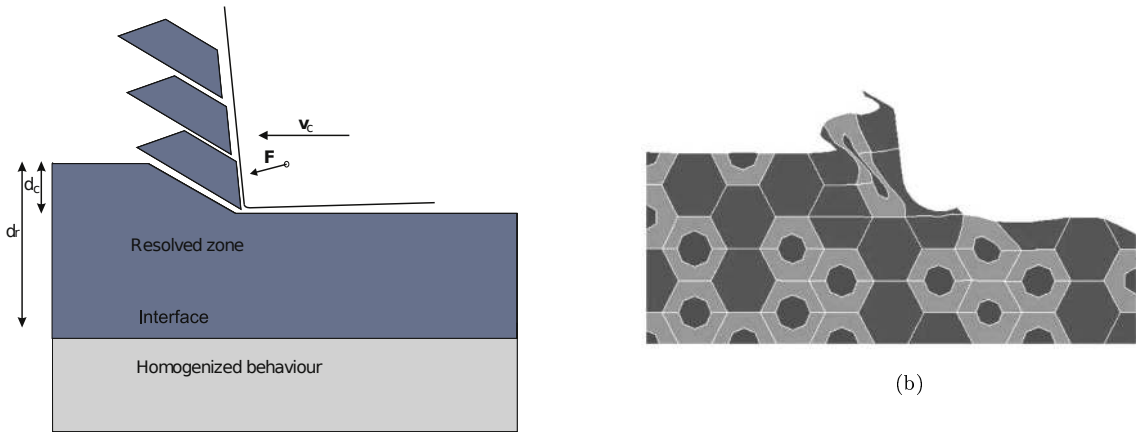

(a) (b)

Figure 22: Machining simulations with discrete microstructure: (a) principal model (from [75]) and (b) results (from [20])

presented in [53]: cleavage was modeled by a cohesive zone in combination with a nonlocal extension of the GTN model for ductile behavior of the bulk material. This model predicts in accordance with experimental findings (compare Section 2.4.1), that for high void volume fractions, being representative for the graphite content in NCI, the crack may propagate stably by cleavage in the upper ductile-brittle transition region. A modified strip yield model, which has certain similarities with a cohesive zone, was used in [133] to simulate fatigue crack growth in NCI including the known overload effects.

5.3 Machining simulations

Machining applications are another field, where the microstructural length scales become important, because the radius of the cutting tool tip lies typically in the range of a few microns. Especially for NCI, typical cutting depths are in the range of the distance between neighboring graphite particles. That is why simulations with discretely resolved microstructure in the cutting zone were performed by Chuzhoy et al. [20–22] and Ljustina et al. [75]. In a certain distance to the cutting zone a homogenized description of the material is sufficient as shown in Figure 22, similar to fracture simulations with discrete microstructure (compare Figure 14). For certain reasons, machining simulations with discrete microstructure are even more ambitious than corresponding fracture simulations. Firstly, in contrast to the process zone of (mode-I dominated) fracture, a low stress triaxiality is found in the shear-dominated cutting zone. Thus, the graphite particle has to be incorporated in the simulations with its elastic and inelastic properties. Secondly, the separation of the metallic matrix, dismissed as "secondary damage" in fracture simulations, is the explicit aim of machining and must thus be incorporated in the simulations. And thirdly, for practically relevant applications, effects of strain-rate and local heating and thus temperature dependence of all relevant parameters cannot be neglected.

Maybe due to these difficulties, only 2D models were employed until now in the cited studies describing all constituents within the framework of simple materials (with the related pathological mesh dependency). An intensive exchange of experience and knowledge between simulations of machining and fracture of NCI, which did not take place yet, will surely be advantageous.

6 Summary and conclusions

Nodular cast iron (NCI) is a widely used iron alloy with nodular graphite particles embedded into the metallic matrix. Strength and toughness of this material compare to many grades of steel. However, experiments show also that due to its microstructural inhomogeneity, NCI exhibits some specific effects which differ from typical steels. This is for instance the tension-compression asymmetry of the yield behavior or the fact that the graphite particles dominate the ductile mechanism of failure. This dominance goes so far that the initiation of competing secondary mechanisms on the microscale has a considerably lower influence on the macroscopic behavior than known from steels. For instance in steels a macroscopic R-curve behavior is associated with the ductile mechanism and thus the macroscopic behavior itself is often denoted as ductile then. However, NCI can exhibit a macroscopic R-curve behavior despite cleavage on the microscale. Also the interaction of crack closure and ductile mechanism under cyclic loading is very complex. For this reason it is at first highly recommendable for NCI to distinguish between macroscopic behavior and mechanisms on the microscale. Secondly, modeling can contribute significantly to the understanding and prediction of the complex interactions of the micromechanisms.

That is why in the present paper an overview of the strategies for modeling of the mechanical behavior of NCI was given. The models applied to NCI in the literature can be classified according to several criteria. One point is whether the material behavior is described in a homogenized way or whether the microstructure is resolved discretely in more or less detail. Classically, homogenized models are applied to engineering structures capturing microscopic mechanisms only in a relatively rough way, whereas models with discrete microstructure serve for the basic understanding of mechanisms. However, with the computing capacities available today, models with discretely resolved microstructure are becoming more and more interesting to direct engineering applications. This applies especially to engineering structures made of NCI where not only the local deformation state but additionally the microstructure differs significantly due to the casting process.

Regarding models with discrete microstructure, cell models are by far the best investigated ones. With such models the influences of the representation of the graphite, of the grain structure (content of ferrite and pearlite/"bull's eye structure") and of secondary voids was studied for NCI under monotonous and cyclic loading under different stress triaxialities. Cell models often serve as a bridge for calibrating homogenized models. However, in situations where gradients appear over distances comparable to microstructural length scales, i.e. for NCI the mean distance between graphite particles, classical homogenized models reach their limits. Resolving the microstructure discretely in such situations in relevant regions is a suitable and today practicable way to overcome this problem. In literature this was done successfully for simulations of fracture and machining processes of NCI, where the microstructure needs to be resolved only within a relatively small region of interest. It will be a promising but challenging task to transfer the achievements of cell models like representation of graphite, grains, secondary damage, etc. to simulations of fracture and machining with resolved microstructure. In close collaboration with experimentalists, such simulations may contribute considerably to improve both the qualitative understanding of the specific mechanisms of NCI and the quantitative predictions thereof.

One point that should, however, not be forgotten is that more detailed models of the micromechanical processes mostly require also more parameters like elastic-plastic parameters of all constituents or interface properties. In the cited papers, mainly two strategies were employed to identify these parameters. The first strategy is to extract parameters directly from tests on pure bulk material of the respective constituents like ferrite and pearlite. Alternatively, inverse parameter identification strategies were employed to identify parameters from tests on the "composite" NCI. The latter strategy requires of course an experimental database of sufficient extent. Available results in literature suggest that the elastic-plastic parameters (Young's modulus, yield stress, hardening exponent, etc.) of constituents can reliably be determined from tests on the individual bulk material. That is why this direct strategy should be employed were possible and inverse procedures should be limited to those few parameters which cannot be measured directly. In any case, if an inverse procedure is necessary, a sensitivity analysis on the effect of changes of respective parameters should be performed with the models in advance in

order to identify firstly the relevant parameters and secondly suitable experimental setups to determine them.

An interesting task for the future is also whether the modeling achievements made for NCI can be transferred to cast irons with non-nodular graphite particles (vermicular or lamellar ones). A recent study on this topic [80] indicates that correct representations of the mechanical behavior of the graphite is even more important as well of the statistics of shape and orientation of the graphite particles leads to a dramatically increased computational effort even for macroscopically homogeneous loading conditions. Predicting fracture toughness values for cast iron with vermicular or lamellar graphite from the microstructure may be a very demanding task for future work. Furthermore, also for NCI the role of the graphite particles in shear dominated states or under cyclic loading requires further research. Regarding cyclic loading and fatigue, it will become possible in the near future to simulate the micromechanical processes in NCI cycle by cycle for larger numbers of loading cycles that are relevant to engineering applications.

Acknowledgements

The authors thank Sebastian Henkel, Peter Hübner, Joachim Ohser, and Marcel Selent for fruitful discussions. Furthermore, the financial support of the Deutsche Forschungsgemeinschaft (DFG) for several projects concerning NCI is gratefully acknowledged.

References

[1] Aoki, S., Kishimoto, K., Takeya, A., Sakata, M., 1984. Effects of microvoids on crack blunting and initiation in ductile materials. Int. J. Fracture. 24 (4), 267–278.

[2] Aravas, N., McMeeking, R. M., 1985. Finite element analysis of void growth near a blunting crack tip. J. Mech. Phys. Solids. 33 (1), 25–49.

[3] Aravas, N., McMeeking, R. M., 1985. Microvoid growth and failure in the ligament between a hole and a blunt crack tip. Int. J. Fracture. 29 (1), 21–38.

[4] ASTM A536, 2009. Standard specification for ductile iron castings.

[5] Baer, W., 2014. Advanced fracture mechanics testing of DCI – a key to valuable toughness data. Int. J. Metalcast. 8 (2), 25–34.

[6] Baer, W., 2014. Performance of modern DCI materials – investigation of microstructural, temperature and loading rate effects on mechanical and fracture mechanical properties. Mater. Sci. Forum. 783, 2244–2249.

[7] Baer, W., Pusch, G., 1995. Investigation of fracture mechanical behaviour of nodular cast iron and welded joints with parent-material-like weld metal. In: Reuter, W. G., Underwood, J. H., Newman, J. C. (Eds.), Fracture Mechanics. Vol. 26 of STP. ASTM, Philadelphia, pp. 361–375.

[8] Baer, W., Wossidlo, P., Abbasi, B., Cassau, M., Häcker, R., Kossert, R., 2009. Large scale testing and statistical analysis of dynamic fracture toughness of ductile cast iron. Eng. Fract. Mech. 76 (8), 1024 – 1036.

[9] Bartels, C., Gerhards, R., Hanselka, H., Herfurth, K., Kaufmann, H., Kleinkröger, W., Lampic, M., Löblich, H., Menk, W., Pusch, G., Schmidt, T., Schütt, K.-H., Tölke, P., Warnke, E. P., 2007. Gusseisen mit Kugelgraphit: Herstellung — Eigenschaften — Anwendung. konstruieren + giessen 32, 1–101.

[10] Benzerga, A. A., Leblond, J.-B., 2010. Ductile fracture by void growth to coalescence. Adv. Appl. Mech. 44, 169–305.

[11] Berdin, C., Dong, M., Prioul, C., 2001. Local approach of damage and fracture toughness for nodular cast iron. Eng. Fract. Mech. 68 (9), 1107–1117.

[12] Beremin, F. M., 1983. A local criterion for cleavage fracture of a nuclear pressure vessel steel. Metall. Mater. Trans. A. 14A, 2277–2287.

[13] Berger, C., Blauel, J. G., Hodulak, L., Pyttel, B., 2005. FKM Guideline Fracture Mechanics Proof of Strength for Engineering Components. VDMA Verlag GmbH, Frankfurt/Main.

[14] Bernauer, G., Brocks, W., 2002. Micro-mechanical modelling of ductile damage and tearing – results of a european numerical round robin. Fatigue. Fract. Eng. M. 25 (4), 363–384.

[15] Berto, F., Lazzarin, P., Tovo, R., 2014. Multiaxial fatigue strength of severely notched cast iron specimens. Int. J. Fatigue. 67, 15 – 27, multiaxial Fatigue 2013.

[16] Besson, J., 2010. Continuum models of ductile fracture: A review. Int. J. Damage. Mech. 19 (1), 3–52.

[17] Bonora, N., Ruggiero, A., 2005. Micromechanical modeling of ductile cast iron incorporating damage. part I: Ferritic ductile cast iron. Int. J. Solids. Struct. 42 (5-6), 1401–1424.

[18] Brocks, W., Hao, S., Steglich, D., 1996. Micromechanical modelling of the damage and toughness behaviour of nodular cast iron materials. J. Phys. VI. 6 (C6), 43–52.

[19] Cavallini, M., Bartolomeo, O. D., Iacoviello, F., 2008. Fatigue crack propagation damaging micromechanisms in ductile cast irons. Eng. Fract. Mech. 75 (3–4), 694–704, international Conference of Crack Paths.

[20] Chuzhoy, L., DeVor, R. E., Kapoor, S. G., 2003. Machining simulation of ductile iron and its constituents, part 2: Numerical simulation and experimental validation of machining. J. Manuf. Sci. Eng. 125 (2), 192–201.

[21] Chuzhoy, L., DeVor, R. E., Kapoor, S. G., Bammann, D. J., 2002. Microstructure-level modeling of ductile iron machining. J. Manuf. Sci. Eng. 124 (2), 162–169.

[22] Chuzhoy, L., DeVor, R. E., Kapoor, S. G., Beaudoin, A. J., Bammann, D. J., 2003. Machining simulation of ductile iron and its constituents, part 1: Estimation of material model parameters and their validation. J. Manuf. Sci. Eng. 125 (2), 181–191.

[23] Collini, L., Nicoletto, G., 2005. Determination of the relationship between microstructure and constitutive behaviour of nodular cast iron with a unit cell model. J. Strain. Anal. Eng. 40 (2), 107–116.

[24] Collini, L., Pirondi, A., 2014. Fatigue crack growth analysis in porous ductile cast iron microstructure. Int. J. Fatigue. 62, 258–265.

[25] Costa, N., Machado, N., Silva, F., 2010. A new method for prediction of nodular cast iron fatigue limit. Int. J. Fatigue. 32 (7), 988 – 995.

[26] Dahlberg, C. F., Öberg, M., Faleskog, J., 2014. Continuum modeling of nodular cast iron using a porous plastic model with pressure-sensitive matrix – experiments, model calibration & verification. Tech. rep., KTH Royal Institute of Technology, School of Engineering Science, Department of Solid Mechanics, Stockholm, Sweden.

[27] Dahlberg, M., 1997. Micromechanical modelling of nodular cast iron, a composite material. Int. J. Cast. Metal. Res. 9 (6), 319–329.

[28] Dahlberg, M., 2004. Fatigue crack propagation in nodular graphite cast iron. Int. J. Cast Met. Res. 17 (1), 29–37.

[29] Devaux, J., Gologanu, M., Leblond, J. B., Perrin, G., 1997. On continued void growth in ductile metals subjected to cyclic loadings. In: Willis, J. (Ed.), IUTAM Symposium on Nonlinear Analysis of Fracture. Vol. 49 of Solid Mechanics and its Applications. Kluwer Academic Publishers, Dordrecht / Boston / London, pp. 299–310.

[30] Dong, M., Prioul, C., François, D., 1997. Damage effect on the fracture toughness of nodular cast iron: Part-II. damage zone characterization ahead of a crack tip. Metall. Mater. Trans. A. 28 (11), 2255–2262.

[31] Dong, M., Prioul, C., François, D., 1997. Damage effect on the fracture toughness of nodular cast iron: PartI. damage characterization and plastic flow stress modeling. Metall. Mater. Trans. A. 28 (11), 2245–2254.

[32] Emrich, A., Mühlich, U., Kuna, M., Ludwig, A., Trubitz, P., 2007. Indirect measuring of crack growth by means of a key-curve-method in pre-cracked Charpy specimens made of nodular cast iron. Int. J. Fracture. 145 (1), 47–61.

[33] EN-1563, 2011. Spheroidal graphite cast irons.

[34] Endo, M., Yanase, K., 2014. Effects of small defects, matrix structures and loading conditions on the fatigue strength of ductile cast irons. Theor. Appl. Fract. Mec. 69, 34 – 43.

[35] Eufinger, J., Heinrietz, A., Bruder, T., Hanselka, H., 2011. Microstructure based fatigue analysis of cast components under variable amplitude loading. Materialwiss. Werkst. 42 (10), 866–873.

[36] Fabrègue, D., Pardoen, T., 2008. A constitutive model for elastoplastic solids containing primary and secondary voids. J. Mech. Phys. Solids. 56 (3), 719–741.

[37] Fischer, G., Nellesen, J., Anar, N., Ehrig, K., Riesemeier, H., Tillmann, W., 2013. 3D analysis of micro-deformation in VHCF-loaded nodular cast iron by μCT. Mat. Sci. Eng. A-Struct. 577, 202–209.

[38] Fritzen, F., Forest, S., Böhlke, T., Kondo, D., Kanit, T., 2012. Computational homogenization of elasto-plastic porous metals. Int. J. Plasticity. 29, 102–119.

[39] Germann, H., Starke, P., Eifler, D., 2012. Resistivity-based evaluation of the fatigue behavior of cast irons. Metall. Mater. Trans. A. 43 (8), 2792–2798.

[40] Ghahremaninezhad, A., Ravi-Chandar, K., 2012. Deformation and failure in nodular cast iron. Acta. Mater. 60 (5), 2359–2368.

[41] Gilles, P., Jullien, B., Mottet, G., 1992. Analysis of cyclic effects on ductile tearing strength by a local approach of fracture. Advances in Fracture/Damage Models for the Analysis of Engineering Problems, 269–284.

[42] Gologanu, M., Leblond, J., Perrin, G., Devaux, J., 1997. Recent extensions of Gurson's model for porous ductile metals. In: Suquet, P. (Ed.), Continuum micromechanics. No. 377 in CISM Courses And Lectures: International Centre For Mechanical Sciences Series. Springer-Verlag, New York, pp. 61–130.

[43] Guillemer-Neel, C., Bobet, V., Clavel, M., 1999. Cyclic deformation behaviour and Bauschinger effect in ductile cast iron. Mat. Sci. Eng. A-Struct. 272 (2), 431–442.

[44] Guillemer-Neel, C., Feaugas, X., Clavel, M., 2000. Mechanical behavior and damage kinetics in nodular cast iron: Part I. damage mechanisms. Metall. Mater. Trans. A. 31 (12), 3063–3074.

[45] Guo, T. F., Faleskog, J., Shih, C. F., 2008. Continuum modeling of a porous solid with pressure-sensitive dilatant matrix. J. Mech. Phys. Solids. 56 (6), 2188–2212.

[46] Gurson, A. L., 1977. Continuum theory of ductile rupture by void nucleation and growth: Part I – yield criteria and flow rules for porous ductile media. J. Eng. Mater-T. Asme. 99 (1), 2–15.

[47] Hanisch, K.-H., Stoyan, D., 1981. Stereological estimation of the radial distribution function of centres of spheres. J. Microsc. 122 (2), 131–141.

[48] Henkel, S., Hübner, P., Pusch, G., 2008. Zyklisches Risswachstumsverhalten von Gusseisenwerkstoffen – statistische Aufbereitung für die Nutzung mit dem Berechnungsprogramm ESACRACK. konstruieren + giessen 33, 41–43.

[49] Hjelm, H. E., 1994. Yield surface for grey cast iron under biaxial stress. J. Eng. Mater. Technol. 116 (2), 148–154.

[50] Hübner, P., Schlosser, H., Pusch, G., Biermann, H., 2007. Load history effects in ductile cast iron for wind turbine components. Int. J. Fatigue. 29 (9-11), 1788–1796.

[51] Hütter, G., 2013. Multi-scale simulation of crack propagation in the ductile-brittle transition region. Dissertation, TU Bergakademie Freiberg.

[52] Hütter, G., Linse, T., Mühlich, U., Kuna, M., 2013. Simulation of ductile crack initiation and propagation by means of a non-local GTN-model under small-scale yielding. Int. J. Solids. Struct. 50, 662–671.

[53] Hütter, G., Linse, T., Roth, S., Mühlich, U., Kuna, M., 2014. A modeling approach for the complete ductile-brittle transition region: Cohesive zone in combination with a non-local Gurson-model. Int. J. Fracture. 185, 129–153.

[54] Hütter, G., Zybell, L., Kuna, M., 2014. Micromechanical modeling of crack propagation with competing ductile and cleavage failure. Procedia Mater. Sci. 3, 428–433.

[55] Hütter, G., Zybell, L., Kuna, M., 2014. Size effects due to secondary voids during ductile crack propagation. Int. J. Solids. Struct. 51 (3–4), 839–847.

[56] Hütter, G., Zybell, L., Kuna, M., 2015. Micromechanical modeling of crack propagation in nodular cast iron with competing ductile and cleavage failure. Eng. Fract. Mech.In press.

[57] Hütter, G., Zybell, L., Mühlich, U., Kuna, M., 2012. Ductile crack propagation by plastic collapse of the intervoid ligaments. Int. J. Fracture. 176, 81–96.

[58] Hütter, G., Zybell, L., Mühlich, U., Kuna, M., 2013. Consistent simulation of ductile crack propagation with discrete 3D voids. Comp. Mater. Sci. 80, 61–70.

[59] Iacoviello, F., Di Bartolomeo, O., Di Cocco, V., Piacente, V., 2008. Damaging micromechanisms in ferritic-pearlitic ductile cast irons. Mat. Sci. Eng. A-Struct. 478 (1-2), 181–186.

[60] Iacoviello, F., Di Cocco, V., Rossi, A., Cavallini, M., 2014. Fatigue crack tip damaging micromechanisms in pearlitic ductile cast irons. Fatigue. Fract. Eng. M. 38 (2), 238–245.

[61] ISO 945-1, 2011. Microstructure of cast irons — part 1: Graphite classification by visual analysis.

[62] Kim, J., Gao, X., Srivatsan, T. S., 2003. Modeling of crack growth in ductile solids: a three-dimensional analysis. Int. J. Solids. Struct. 40 (26), 7357–7374.

[63] Kobayashi, T., 2004. Ductile cast iron. In: Strength and Toughness of Materials. Springer, pp. 89–110.

[64] Kobayashi, T., Toda, H., 2001. Fracture in complex microstructures. Mater. Trans. 42 (1), 90–99.

[65] Kobayashi, T., Yamada, S., 1994. Evaluation of static and dynamic fracture toughness in ductile cast iron. Metall. Mater. Trans. A. 25 (11), 2427 – 2437.

[66] Komatsu, S., Shiota, T., Matsuoka, T., Nakamura, K., 1994. Effects of several main factors on ductile-brittle transition behaviors of fracture toughness in SG cast iron. AFS Transactions 102, 121–126.

[67] Koplik, J., Needleman, A., 1988. Void growth and coalescence in porous plastic solids. Int. J. Solids. Struct. 24 (8), 835–853.

[68] Kuna, M., Mühlich, U., Hütter, G., 2014. Entwicklung eines Mehrskalenmodells zur Beschreibung des Bruchverhaltens von GJS-400 bei statischer und stoßartiger Beanspruchung im gesamten Zähigkeitsbereich. Abschlussbericht zum DFG-Vorhaben KU 929/14.

[69] Kuna, M., Sun, D., 1996. Three-dimensional cell model analyses of void growth in ductile materials. Int. J. Fracture. 81 (3), 235–258.

[70] Labrecque, C., Gagné, M., 1998. Review ductile iron: fifty years of continuous development. Can. Metall. Quart. 37 (5), 343 – 378.

[71] Lachambre, J., Réthoré, J., Weck, A., Buffiere, J.-Y., 2015. Extraction of stress intensity factors for 3D small fatigue cracks using digital volume correlation and X-ray tomography. Int. J. Fatigue. 72, 3–10.

[72] Limodin, N., Réthoré, J., Buffière, J., Gravouil, A., Hild, F., Roux, S., 2009. Crack closure and stress intensity factor measurements in nodular graphite cast iron using three-dimensional correlation of laboratory X-ray microtomography images. Acta. Mater. 57 (14), 4090–4101.

[73] Limodin, N., Réthoré, J., Buffière, J., Hild, F., Roux, S., Ludwig, W., Rannou, J., Gravouil, A., 2010. Influence of closure on the 3D propagation of fatigue cracks in a nodular cast iron investigated by X-ray tomography and 3D volume correlation. Acta. Mater. 58 (8), 2957–2967.

[74] Liu, J. H., Hao, X. Y., Li, G. L., Liu, G. S., 2002. Microvoid evaluation of ferrite ductile iron under strain. Mater. Lett. 56 (5), 748–755.

[75] Ljustina, G., Larsson, R., Fagerström, M., 2014. A FE based machining simulation methodology accounting for cast iron microstructure. Finite. Elem. Anal. Des. 80, 1–10.

[76] Martínez, R. A., 2010. Fracture surfaces and the associated failure mechanisms in ductile iron with different matrices and load bearing. Eng. Fract. Mech. 77 (14), 2749–2762.

[77] Mellouli, D., Haddar, N., Köster, A., Toure, A. M.-L., 2011. Thermal fatigue of cast irons for automotive application. Mater. Design. 32 (3), 1508 – 1514.

[78] Memhard, D., Andrieux, F., Sun, D.-Z., Häcker, R., 2011. Development and verification of a material model for prediction of containment safety of exhaust turbochargers. In: 8th European LS-DYNA Users Conference.

[79] Metzger, M., Nieweg, B., Schweizer, C., Seifert, T., 2013. Lifetime prediction of cast iron materials under combined thermomechanical fatigue and high cycle fatigue loading using a mechanism-based model. Int. J. Fatigue. 53, 58–66.

[80] Metzger, M., Seifert, T., 2015. Computational assessment of the microstructure-dependent plasticity of lamellar gray cast iron - Part I: Methods and microstructure-based models. Int. J. Solids. Struct. 66, 184–193.

[81] Mottitschka, T., Pusch, G., Biermann, H., Zybell, L., Kuna, M., 2012. Influence of graphite spherical size on fatigue behaviour and fracture toughness of ductile cast iron EN-GJS-400-18LT. J. Mater. Res. 103 (1), 87–96.

[82] Münstermann, S., Lian, J., Döbereiner, B., 2015. Über die Ursachen für unterschiedliche Übergangstemperaturen bei der Zähigkeitscharakterisierung in Kerbschlagbiege- und Bruchmechanikversuch. Giesserei.

[83] Nagel, W., Ohser, J., 1988. On the stereological estimation of weighted sphere diameter distributions. Acta Stereol. 7, 17–31.

[84] Needleman, A., Tvergaard, V., 1987. An analysis of ductile rupture modes at a crack tip. J. Mech. Phys. Solids. 35 (2), 151–183.

[85] Needleman, A., Tvergaard, V., 1995. Analysis of a brittle-ductile transition under dynamic shear loading. Int. J. Solids. Struct. 32 (17-18), 2571–2590.

[86] Nicoletto, G., Collini, L., Konečná, R., Bujnová, P., 2005. Strain heterogeneity and damage localization in nodular cast iron microstructures. Mater. Sci. Forum. 482, 255–258.

[87] Nicoletto, G., Collini, L., Konečná, R., Riva, E., May 2006. Analysis of nodular cast iron microstructures for micromechanical model development. Strain 42 (2), 89–96.

[88] Nielsen, K. L., Dahl, J., Tvergaard, V., 2012. Collapse and coalescence of spherical voids subject to intense shearing: studied in full 3D. Int. J. Fracture. 177 (2), 97–108.

[89] Nilsson, K.-F., Blagoeva, D., Moretto, P., 2006. An experimental and numerical analysis to correlate variation in ductility to defects and microstructure in ductile cast iron components. Eng. Fract. Mech. 73 (9), 1133 – 1157.

[90] Nilsson, K.-F., Vokál, V., 2009. Analysis of ductile cast iron tensile tests to relate ductility variation to casting defects and material microstructure. Mat. Sci. Eng. A-Struct. 502 (1–2), 54 – 63.

[91] Ohser, J., Mücklich, F., 2000. Statistical analysis of microstructures in materials science. Wiley, Chichester.

[92] Palin-Luc, T., Lasserre, S., Berard, Y., 1998. Experimental investigation on the significance of the conventional endurance limit of a spheroidal graphite cast iron. Fatigue. Fract. Eng. M. 21 (2), 191–200.

[93] Pardoen, T., Hutchinson, J., 2003. Micromechanics-based model for trends in toughness of ductile metals. Acta. Mater. 51 (1), 133–148.

[94] Petti, J. P., Dodds, Jr., R. H., 2005. Ductile tearing and discrete void effects on cleavage fracture under small-scale yielding conditions. Int. J. Solids. Struct. 42 (13), 3655–3676.

[95] Pineau, A., 2008. Modeling ductile to brittle fracture transition in steels — micromechanical and physical challenges. Int. J. Fracture. 150 (1-2), 129–156.

[96] Pusch, G., Henkel, S., Biermann, H., Hübner, P., Ludwig, A., Trubitz, P., Mottitschka, T., Krüger, L., 2015. Determination of fracture mechanics parameters for cast iron materials under static, dynamic and cyclic loading. In: Hütter, G., Zybell, L. (Eds.), Recent Trends in Fracture and Damage Mechanics. Springer.

[97] Rabold, F., Kuna, M., 2005. Cell model simulation of void growth in nodular cast iron under cyclic loading. Comp. Mater. Sci. 32 (3-4), 489–497.

[98] Rausch, T., Beiss, P., Broeckmann, C., Lindlohr, S., Weber, R., 2010. Application of quantitave image analysis of graphite structures for the fatigue strength estimation of cast iron materials. Procedia Eng. 2 (1), 1283 – 1290.

[99] Ristinmaa, M., 1997. Void growth in cyclic loaded porous plastic solid. Mech. Mater. 26 (4), 227–245.

[100] Ritchie, R. O., Knott, J. F., Rice, J. R., 1973. On the relationship between critical tensile stress and fracture toughness in mild steel. J. Mech. Phys. Solids. 21 (6), 395–410.

[101] Rosenfield, A., Ahmad, J., Cialone, H., Landow, M., Mincer, P., Papaspyropoulos, V., 1989. Crack arrest toughness of nodular iron. Nucl. Eng. Des. 116 (2), 161–170.

[102] Salzbrenner, R., 1987. Fracture toughness behaviour of ferritic ductile cast iron. J. Mater. Sci. 22, 2135–2147.

[103] Schwalbe, K.-H., Scheider, I., Cornec, A., 2013. Guidelines for Applying Cohesive Models to the Damage Behavior of Engineering Materials and Structures. Springer.

[104] Seifert, T., Maier, G., Uihlein, A., Lang, K.-H., Riedel, H., 2010. Mechanism-based thermomechanical fatigue life prediction of cast iron. part II: Comparison of model predictions with experiments. Int. J. Fatigue. 32 (8), 1368–1377.

[105] Seifert, T., Riedel, H., 2010. Mechanism-based thermomechanical fatigue life prediction of cast iron. part I: Models. Int. J. Fatigue. 32 (8), 1358–1367.

[106] Seifert, T., Schmidt, I., 2009. Plastic yielding in cyclically loaded porous materials. Int. J. Plasticity. 25 (12), 2435 – 2453.

[107] Shirani, M., Härkegård, G., 2011. Casting defects and fatigue behaviour of ductile cast iron for wind turbine components: A comprehensive study. Materialwiss. Werkst. 42 (12), 1059–1074.

[108] Smirnova, L. N., Shcheglyuk, N., 1989. Features of failure for ferritic cast iron with spheroidal graphite. Met. Sci. Heat. Treat. 31 (4), 255–258.

[109] Steglich, D., Brocks, W., 1998. Micromechanical modelling of damage and fracture of ductile materials. Fatigue. Fract. Eng. M. 21 (10), 1175–1188.

[110] Steglich, D., Pirondi, A., Bonora, N., Brocks, W., 2005. Micromechanical modelling of cyclic plasticity incorporating damage. Int. J. Solids. Struct. 42 (2), 337–351.

[111] Thomason, P., 1985. Three-dimensional models for the plastic limit-loads at incipient failure of the intervoid matrix in ductile porous solids. Acta. Metall. Mater. 33 (6), 1079–1085.

[112] Tian, R., Chan, S., Tang, S., Kopacz, A. M., Wang, J.-S., Jou, H.-J., Siad, L., Lindgren, L.-E., Olson, G. B., Liu, W. K., 2010. A multiresolution continuum simulation of the ductile fracture process. J. Mech. Phys. Solids. 58 (10), 1681–1700.

[113] Trubitz, P., Winkler, H.-P., Hüggenberg, R., Ludwig, A., Pusch, G., 2013. Effect of the pearlite content of ferritic cast iron material on the crack resistance behaviour under dynamic load. In: Proceedings of 13th International Conference on Fracture.

[114] Tvergaard, V., 1981. Influence of voids on shear band instabilities under plane strain conditions. Int. J. Fracture. 17 (4), 389–407.

[115] Tvergaard, V., 1982. On localization in ductile materials containing spherical voids. Int. J. Fracture. 18 (4), 237–252.

[116] Tvergaard, V., 1989. Material failure by void growth to coalescence. Adv. Appl. Mech. 27, 83–151.

[117] Tvergaard, V., 2009. Behaviour of voids in a shear field. Int. J. Fracture. 158 (1), 41–49.

[118] Tvergaard, V., Hutchinson, J. W., 2002. Two mechanisms of ductile fracture: void by void growth versus multiple void interaction. Int. J. Solids. Struct. 39 (13-14), 3581–3597.

[119] Tvergaard, V., Needleman, A., 1984. Analysis of the cup-cone fracture in a round tensile bar. Acta. Metall. Mater. 32 (1), 157–169.

[120] Tvergaard, V., Needleman, A., 1993. An analysis of the brittle-ductile transition in dynamic crack growth. Int. J. Fracture. 59 (1), 53–67.

[121] Tvergaard, V., Needleman, A., 2006. Three dimensional microstructural effects on plane strain ductile crack growth. Int. J. Solids. Struct. 43 (20), 6165–6179.

[122] Velichko, A., Holzapfel, C., Siefers, A., Schladitz, K., Mücklich, F., 2008. Unambiguous classification of complex microstructures by their three-dimensional parameters applied to graphite in cast iron. Acta Materialia 56 (9), 1981 – 1990.

[123] Verdu, C., Adrien, J., Buffière, J., 2008. Three-dimensional shape of the early stages of fatigue cracks nucleated in nodular cast iron. Mat. Sci. Eng. A-Struct. 483, 402–405.

[124] Weidner, A., Mottitschka, T., Biermann, H., Henkel, S., 2013. Determination of stretch zone width and height by powerful 3D SEM imaging technology. Eng. Fract. Mech. 108, 294 – 304.

[125] Winkler, H.-P., Hüggenberg, R., Ludwig, A., Pusch, G., Trubitz, P., 2009. Determination and definition of fracture toughness of dynamically loaded ductile cast iron. In: Proceedings of 12th International Conference on Fracture. Ottawa.

[126] Wolfensberger, S., 1986. Bruchzähigkeit von Gusseisen. Dissertation, ETH Zürich.

[127] Xia, L., Shih, C. F., 1995. Ductile crack growth–I. a numerical study using computational cells with microstructurally-based length scales. J. Mech. Phys. Solids. 43 (2), 233–259.

[128] Xue, H., Bayraktar, E., Bathias, C., 2008. Damage mechanism of a nodular cast iron under the very high cycle fatigue regime. J. Mater. Process. Tech. 202 (1–3), 216 – 223.

[129] Zambrano, H., Härkegård, G., Stärk, K., 2012. Fracture toughness and growth of short and long fatigue cracks in ductile cast iron EN-GJS-400-18-LT. Fatigue. Fract. Eng. M. 35 (4), 374–388.

[130] Zhang, K. S., Bai, J. B., François, D., 1999. Ductile fracture of materials with high void volume fraction. Int. J. Solids. Struct. 36 (23), 3407–3425.

[131] Zybell, L., Chaves, H., Kuna, M., Mottitschka, T., Pusch, G., Biermann, H., 2012. Optical in situ investigations of overload effects during fatigue crack growth in nodular cast iron. Eng. Fract. Mech. 95, 45–56.

[132] Zybell, L., Hütter, G., Linse, T., Mühlich, U., Kuna, M., 2014. Size effects in ductile failure of porous materials containing two populations of voids. Eur. J. Mech. A-Solid. 45, 8–19.

[133] Zybell, L., Selent, M., Hübner, P., Kuna, M., 2014. Overload effects during fatigue crack growth in nodular cast iron - simulation with an extended strip-yield model. Procedia Mater. Sci. 3, 221–226.

[134] Čanžar, P., Tonković, Z., Kodvanj, J., 2012. Microstructure influence on fatigue behaviour of nodular cast iron. Mat. Sci. Eng. A-Struct. 556, 88–99.